Chlorine partitioning near the polar vortex boundary observed with ground-based FTIR and satellites at Syowa Station, Antarctica in 2007 and 2011

Hideaki Nakajima[1,2], Isao Murata[2], Yoshihiro Nagahama[1], Hideharu Akiyoshi[1], Kosuke Saeki[2,3], Takeshi Kinase[4], Masanori Takeda[2], Yoshihiro Tomikawa[5,6], and Nicholas B. Jones[7]

[1]National Institute for Environmental Studies, Tsukuba, Ibaraki, 305-8506, Japan
[2]Graduate School of Environmental Studies, Tohoku University, Sendai, Miyagi, 980-8572, Japan
[3]now at Weathernews Inc., Chiba, 261-0023, Japan
[4]Meteorological Research Institute, Tsukuba, Ibaraki, 305-0052, Japan
[5]National Institute of Polar Research, Tachikawa, Tokyo, 190-8518, Japan
[6]The Graduate University for Advanced Studies, Tachikawa, Tokyo, 190-8518, Japan
[7]University of Wollongong, Wollongong, New South Wales, 2522, Australia

Correspondence to: Hideaki Nakajima (nakajima@nies.go.jp)

Abstract.

We retrieved lower stratospheric vertical profiles of O_3, HNO_3, and HCl from solar spectra taken with a ground-based Fourier-Transform infrared spectrometer (FTIR) installed at Syowa Station, Antarctica (69.0ºS, 39.6ºE) from March to December 2007 and September to November 2011. This was the first continuous measurements of chlorine species throughout the ozone hole period from the ground in Antarctica. We analyzed temporal variation of these species combined with ClO, HCl, and HNO_3 data taken with the Aura/MLS (Microwave Limb Sounder) satellite sensor, and $ClONO_2$ data taken with the Envisat/MIPAS (The Michelson Interferometer for Passive Atmospheric Sounding) satellite sensor at 18 and 22 km over Syowa Station. HCl and $ClONO_2$ decrease occurred at both 18 and 22 km, and soon $ClONO_2$ was almost depleted in early winter. When the sun returned to Antarctica in spring, enhancement of ClO and gradual O_3 destruction were observed. During the ClO enhanced period, negative correlation between ClO and $ClONO_2$ was observed in the time-series of the data at Syowa Station. This negative correlation was associated with the distance between Syowa Station and the inner edge of the polar vortex. We used MIROC3.2 Chemistry-Climate Model (CCM) results to see the comprehensive behavior of chlorine and related species inside the polar vortex and the edge region in more detail. From CCM model results, rapid conversion of chlorine reservoir species (HCl and $ClONO_2$) into Cl_2, gradual conversion of Cl_2 into Cl_2O_2, increase of ClO when sunlight became available, and conversion of ClO into HCl, was successfully reproduced. HCl decrease in the winter polar vortex core continued to occur due to the transport of $ClONO_2$ from the subpolar region to higher latitudes, providing a flux of $ClONO_2$ from more sunlit latitudes into the polar vortex. Temporal variation of chlorine species over Syowa Station was affected by both heterogeneous chemistry related to Polar Stratospheric Cloud (PSC) occurrence deep inside the polar vortex, and transport of an NO_x-rich airmass from lower latitudinal polar vortex boundary region which can produce additional $ClONO_2$ by reaction of ClO with NO_2. The deactivation pathways from active chlorine into reservoir species (HCl and/or $ClONO_2$) were found to

be highly dependent on the availability of ambient O_3. At an altitude where most ozone was depleted in Antarctica (18 km), most ClO was converted to HCl. However, at an altitude where there were some O_3 available (22 km), additional increase of $ClONO_2$ from pre-winter value can occur, similar to the case as in the Arctic.

1. Introduction

Discussion of the detection of "recovery" of the Antarctic ozone hole as the result of chlorofluorocarbon (CFC) regulations has been attracting attention. The occurrence of the Antarctic ozone hole is considered to continue at least until the middle of this century. The world's leading Chemistry-Climate Models (CCMs) indicate that the multi-model mean time series of the springtime Antarctic total column ozone will return to 1980 levels shortly after mid-century (about 2060) (WMO, 2019). In fact, the recovery time predicted by CCMs has large uncertainty, and observed ozone hole magnitude also shows year-to-year variability. Although Solomon et al. (2016) and de Laat et al. (2017) reported signs of healing in the Antarctic ozone layer only in September month, there is no statistically conclusive report on the Antarctic ozone hole recovery (Yang et al., 2008; Kuttippurath et al, 2010; WMO, 2019).

To understand ozone depletion processes in polar regions, understanding of the behavior and partitioning of active chlorines (ClO_x=Cl+Cl_2+ClO+ClOO+Cl_2O_2+HOCl+$ClNO_2$) and chlorine reservoirs (HCl and $ClONO_2$) are crucial. Recently, the importance of $ClONO_2$ was reviewed by von Clarmann and Johansson (2018). Chlorine reservoir is converted to active chlorine that destroys ozone on polar stratospheric clouds (PSCs) and/or cold binary sulphate through heterogeneous reactions:

$ClONO_2$ (g) + HCl (s, l) → Cl_2 (g) + HNO_3 (R1)

$ClONO_2$ (g) + H_2O (s, l) → HOCl (g) + HNO_3 (R2)

where g, s, and l represent the gas, solid, and liquid phases, respectively (Solomon et al., 1986; Solomon, 1999; Drdla and Müller, 2012, Wegner et al., 2012; Nakajima et al., 2016).

Heterogeneous reactions;

N_2O_5 (g) + HCl (s, l) → $ClNO_2$ (g) + HNO_3 (R3)

HOCl (g) + HCl (s, l) → Cl_2 (g) + H_2O (R4)

are responsible for additional chlorine activation. When solar illumination is available, Cl_2, HOCl, and $ClNO_2$ are photolyzed to produce chlorine atoms by reactions:

Cl_2 + hv → Cl + Cl (R5)

HOCl + hv → Cl + OH (R6)

$ClNO_2$ + hv → Cl + NO_2. (R7)

The yielded chlorine atoms then start to destroy ozone catalytically through reactions (Canty et al., 2016):

Cl + O_3 → ClO + O_2 (R8)

ClO + ClO + M → Cl_2O_2 + M (R9)

$Cl_2O_2 + hv \rightarrow Cl + ClOO$ (R10)

$ClOO + M \rightarrow Cl + O_2 + M.$ (R11)

There are three types of PSCs, i.e., nitric acid trihydrate (NAT), supercooled ternary solution (STS), and ice PSCs. When the stratospheric temperatures get warmer than NAT PSC saturation temperature (about 195 K at 50 hPa) and no PSCs are present, deactivation of chlorine starts to occur. Re-formation of $ClONO_2$ and HCl mainly occurs through reactions:

$ClO + NO_2 + M \rightarrow ClONO_2 + M$ (R12)

$Cl + CH_4 \rightarrow HCl + CH_3.$ (R13)

$CH_2O + Cl \rightarrow HCl + CHO$ (R14)

The re-formation of $ClONO_2$ by reaction (R12) from active chlorine is much faster than that of HCl by reactions (R13) and (R14), if enough NO_x are available (Mellqvist et al., 2002; Dufour et al., 2006). But the formation rates of $ClONO_2$ and HCl are also related to ozone concentration. Grooß et al. (1997) showed that HCl increases more rapidly in the Antarctic polar vortex than in the Arctic polar vortex due to lower ozone concentrations in the Antarctic polar vortex. Low ozone reduces the rate of reaction (R8), and then Cl/ClO ratio becomes high. Low ozone also reduces the rate of the following reaction:

$NO + O_3 \rightarrow NO_2 + O_2.$ (R15)

This makes NO/NO_2 ratio high and increases Cl/ClO ratio by the following reaction:

$ClO + NO \rightarrow Cl + NO_2.$ (R16)

High Cl/ClO ratio leads to rapid HCl formation by reactions (R13) and (R14), and reduces the formation ratio of $ClONO_2$ by reaction (R12).

The processes of deactivation of active chlorine are different between typical conditions in the Antarctic and those in the Arctic. In the Antarctic, the temperature cools below the NAT PSC formation threshold (about 195 K at 50 hPa) in the whole area of the polar vortex in most years, and almost complete denitrification and chlorine activation occur (WMO, 2007), followed by severe ozone depletion in spring. In the chlorine reservoir recovery phase, HCl is mainly formed by reaction (R13) due to the lack of ozone (typically less than 0.5 ppmv) by the mechanism described in the previous paragraph (Grooß et al., 2011).

On the other hand, in the Arctic, typically less PSC formation occurs in the polar vortex due to generally higher stratospheric temperatures (~10-15K in average) compared with that of Antarctica. Then only partial denitrification and chlorine activation occur in some years (Manney et al., 2011; WMO, 2014). In this case, some ozone and NO_2 are available in the chlorine reservoir recovery phase. Therefore, the $ClONO_2$ amount becomes sometimes higher than that of HCl after PSCs have disappeared due to the rapid reaction (R12) (Michelsen et al., 1999; Santee et al., 2003), which results in additional increase of $ClONO_2$ than pre-winter value at the time of chlorine deactivation in spring (von Clarmann et al., 1993; Müller et al., 1994; Oelhaf et al., 1994). In this way, the partitioning of chlorine reservoir in springtime is related to temperature, PSC amounts, ozone, and NO_2 concentrations (Santee et al., 2008; Solomon et al., 2015).

In the polar regions, the ozone and related atmospheric trace gas species have been intensively monitored by several measurement techniques since the discovery of the ozone hole. These measurements consist of direct observations by high-

altitude aircrafts (e.g., Anderson et al., 1989; Ko et al., 1989; Bonne et al., 2000), remote sensing observations by satellites (e.g., Müller et al., 1996; Michelsen et al., 1999; Höpfner et al., 2004; Dufour et al., 2006; Hayashida et al., 2007), remote sensing observations from the ground (e.g., Farmer et al., 1987; Kreher et al., 1996; Solomon et al., 1997; Mellqvist et al., 2002; Blumenstock et al., 2006). Within these observations, ground-based measurements have the characteristic of high temporal resolution. In addition, the Fourier-Transform infrared spectrometer (FTIR) has the capability of measuring several trace gas species at the same time or in a short time interval. In this paper, we show the results of ground-based FTIR observations of O_3 and other trace gas species at Syowa Station in the Antarctic in 2007 and 2011, combined with the satellite measurements of trace gas species by Microwave Limb Sounder onboard the Aura satellite (Aura/MLS) and Michelson Interferometer for Passive Atmospheric Sounding onboard the European Environmental Satellite (Envisat/MIPAS), to show the temporal variation and partitioning of active chlorine (ClO_x) and chlorine reservoirs (HCl, $ClONO_2$) from fall to spring during the ozone hole formation and dissipation period. In order to monitor the appearance of PSCs over Syowa Station, we used the Cloud-Aerosol Lidar with Orthogonal Polarization (CALIOP) data onboard the Cloud-Aerosol Lidar and Infrared Pathfinder Satellite Observations (CALIPSO) satellite. The methods of FTIR and satellite measurements are described in Section 2. The validation of FTIR measurements is described in Section 3. The results of FTIR and satellite measurements and discussion on the behavior of active and inert chlorine species using the MIROC3.2 chemistry-climate model are described in Section 4.

2. Measurements

2.1 FTIR measurements

The Japanese Antarctic Syowa Station (69.0ºS, 39.6ºE) was established in January 1957. Since then, several scientific observations related to meteorology, upper atmospheric physics, glaciology, biology, geology, seismology, etc. have been performed. The ozone hole was first detected by Dobson spectrometer and ozonesonde measurements from Syowa Station in 1982 (Chubachi, 1984) and Halley Bay (Farman et al., 1985). We installed a Bruker IFS-120M high-resolution Fourier-Transform infrared spectrometer (FTIR) in the Observation Hut at Syowa Station in March 2007. This was the second high-resolution FTIR site in Antarctica in operation after New Zealand's Arrival Heights facility at Scott Station (77.8°S, 166.7°E) (Wood et al., 2002; Wood et al., 2004). The IFS-120M FTIR has a wavenumber resolution of 0.0035 cm^{-1}, with two liquid nitrogen cooled detectors (InSb and HgCdTe covering the frequency ranges 2000-5000 and 700-1300 cm^{-1}, respectively), and fed by an external solar tracking system. Since Syowa Station is located at a relatively low latitude (69.0°S) compared with Scott Station (77.8°S), there is an advantage of the short (about one month) polar night period, when we cannot measure atmospheric species using the sun as a light source. Since FTIR measurements at Syowa Station are possible from early spring (late July), FTIR can measure chemical species during ozone hole development. Another advantage of Syowa Station is that the location enables us to measure both inside and outside of the polar vortex, since the station is sometimes located near the

edge of the polar vortex. From March to December 2007, we made in total 78 days of FTIR measurements. Another 19 days of FTIR measurements were performed from September to November 2011. Table 1 shows the days when FTIR measurements were made at Syowa Station with the information inside/boundary/outside of the polar vortex defined by the method described in Section 4 using ERA-Interim reanalysis data.

The retrieval of the FTIR spectra was done with SFIT2 Version 3.92 program (Rinsland et al., 1998; Hase et al., 2004). SFIT2 retrieves a vertical profile of trace gases using an optimal estimation formulation of Rodgers (2000), implemented with a semi-empirical method which was originally developed for microwave measurements (Parrish et al., 1992; Connor et al., 1995). The SFIT2 forward model fully describes the FTIR instrument response, with absorption coefficients calculated using the algorithm of Norton and Rinsland (1991). The atmosphere is constructed with 47 layers from the ground to 100 km, using the FSCATM (Gallery et al., 1983) program for atmospheric ray-tracing to account for refractive bending. The retrieval parameters for each gas are shown in Table 2. Temperature and pressure profiles between 0 and 30 km are taken by the Rawin sonde observations flown from Syowa Station on the same day by the Japanese Meteorological Agency (JMA), while values between 30 and 100 km are taken from the COSPAR International Reference Atmosphere 1986 (CIRA-86) standard atmosphere profile (Rees et al., 1990).

We retrieved vertical profiles of O_3, HCl, and HNO_3 from the solar spectra. We used monthly averaged ozonesondes profiles (0-30 km) and Improve Limb Atmospheric Spectrometer-II (ILAS-II) (Nakajima, 2006; Nakajima et al., 2006; Sugita et al., 2006) profiles (30-100 km) for the a priori of O_3, monthly averaged profiles from ILAS-II for HNO_3 and monthly averaged profiles from HALOE (Anderson et al., 2000) for HCl. Typical averaging kernels of the SFIT2 retrievals for O_3, HNO_3, and HCl are shown in Figures 1(a), (b), and (c), respectively.

2.2 Satellite measurements

The Earth Observing System (EOS) MLS onboard the Aura satellite was launched on 15 July 2004, to monitor several atmospheric chemical species in upper troposphere to mesosphere (Waters et al., 2006). The Aura orbit is sun-synchronous at 705 km altitude with an inclination of 98°, 13:45 ascending (north-going) equator-crossing time, and 98.8-min period. Vertical profiles are measured every ~165 km along the suborbital track, horizontal resolution is ~200-600 km along-track, ~3-10 km across-track, and vertical resolution is ~3-4 km in the lower to middle stratosphere (Froidevaux et al., 2006). ClO, HCl, and HNO_3 profiles used in this study were taken from Aura/MLS version 4.2 data (Liversey et al., 2006; Santee et al., 2011; Ziemke et al., 2011; Liversey et al., 2018). The MLS data was selected whose measurement location is within 300 km radius from Syowa Station and within ±6 hours of the FTIR measurement.

MIPAS is a Fourier transform spectrometer sounding the thermal emission of the earth's atmosphere between 685 and 2410 cm^{-1} (14.6-4.15 μm) in limb geometry (Fischer and Oelhaf, 1996; Fischer et al., 2008). The maximum optical path difference of MIPAS is 20 cm. The field-of-view of the instrument at the tangent points is about 3 km in the vertical and 30 km in the horizontal. In the standard observation mode in one limb-scan, 17 tangent points are observed with nominal altitudes 6, 9, 12, …, 39, 42, 47, 52, 60, and 68 km. In this mode, about 73 limb scans are recorded per orbit. The measurements of

each orbit cover nearly the complete latitude range from about 87°S to 89°N. MIPAS was put on board the Envisat, which was launched on 1 March 2002, and was put into a polar sun-synchronous orbit at an altitude of about 800 km with an inclination of 98.55° (von Clarmann et al., 2003). On its descending node, the satellite crosses the equator at 10:00 local time. Envisat performs 14.3 orbits per day, which results in a good global coverage. $ClONO_2$ profiles which we used in this study were taken from Envisat/MIPAS IMK/IAA version V5R_CLONO2_220 and V5R_CLONO2_222 (Höpfner et al., 2007). The selection criteria of the MIPAS data used in this study are the same as that of Aura/MLS.

The CALIPSO satellite was launched on 28 April 2006. On CALIPSO satellite, CALIOP instrument was on board, to monitor aerosols, clouds, and PSCs (Pitts et al., 2007). CALIOP is a two-wavelength, polarization sensitive lidar that provides high vertical resolution profiles of backscatter coefficient at 532 and 1064 nm, as well as two orthogonal (parallel and perpendicular) polarization components at 532 nm (Winker et al., 2007). In order to monitor the appearance of PSCs over Syowa Station, we used CALIOP PSC data (Pitts et al., 2007; 2009; 2011).

3. Validation of retrieved profiles from FTIR spectra with other measurements

We validated retrieved FTIR profiles of O_3 with ozonesondes, and HNO_3 and HCl with Aura/MLS version 3.3 data (Liversey et al., 2013) for 2007 measurements. We identified the nearest Aura/MLS data from the distance between the Aura/MLS tangent point at 20 km altitude and the point at 20 km altitude for the direction of the sun from Syowa Station at the time of the FTIR measurement. The spatial and temporal collocation criteria used was within 300 km radius and ±6 hours, as stated in Section 2.2. The ozonesonde and Aura/MLS profiles were interpolated onto a 1 km-grid, then smoothed with a 5 km-wide slit function.

Figures 2(a)-(b) show absolute and relative percentage differences of O_3 profiles retrieved from FTIR measurements and those from ozonesonde measurements, respectively, calculated from 14 coincident measurements from September 5 to December 17, 2007. We define the relative percentage difference D as:

$$D\ (\%) = 100 * (\text{FTIR-sonde}) / ((\text{FTIR+sonde})/2). \quad (1)$$

The absolute difference between 15 and 25 km was within -0.02 to 0.40 ppmv. The relative difference D between 15 and 25 km was within -10.4 to +24.4%. The mean relative difference D of O_3 for the altitude of interest in this study (18-22 km) was +6.1%, with the minimum of -10.4% and the maximum of +19.2%. FTIR data agree with validation data within error bars at the altitude of interest. Note that relatively large D values between 16 and 18 km are due to small ozone amount in the ozone hole.

Figures 2(c)-(d) show absolute and percentage differences of HNO_3 profiles retrieved by FTIR measurements and those from Aura/MLS measurements, respectively, calculated from 47 coincident measurements from March 25 to December 20, 2007. The agreement between 15 and 25 km was within -0.56 to +0.57 ppbv. The relative difference D between 15 and 25 km was within -25.5 to +21.9%. The mean relative difference D for HNO_3 for the altitude of interest in this study (18-22 km) was

+13.2%, with the minimum of +0.2% and the maximum of +21.9%. This positive bias of FTIR data is still within the error bars of FTIR measurements. Livesey et al. (2013) showed that Aura/MLS version 3.3 data has no bias within errors (~0.6-0.7 ppbv at pressure level of 100-3.2 hPa) compared with other measurements.

Figures 2(e)-(f) show absolute and relative percentage differences of HCl profiles retrieved by FTIR measurements and those from Aura/MLS measurements, respectively, calculated from 50 coincident measurements from March 25 to December 20, 2007. The agreement between 15 and 25 km was within -0.20 to -0.09 ppbv. The relative difference D between 15 and 25 km was within -34.1 to -3.0%. The mean relative difference D for HCl for the altitude of interest in this study (18-22 km) is -9.7%, with a minimum of -14.6% and a maximum of -3.0%. This negative bias of FTIR data is still within the error bars of FTIR measurements. Moreover, Livesey et al. (2013) showed that Aura/MLS version 3.3 values are systematically greater than HALOE values by 10-15% with a precision of 0.2-0.6% in the stratosphere, which may partly explain the negative bias of FTIR data compared with MLS data.

Table 3 summarizes validation results of FTIR profiles compared with ozonesonde or Aura/MLS measurements, and possible Aura/MLS biases from literature.

4. Results and discussion

4.1 Time series of observed species

Figures 3(a)-(d) show the time series of temperatures at 18 and 22 km over Syowa Station using ERA-Interim data (Dee et al., 2011) for 2007 and 2011. Approximate saturation temperatures for NAT PSC (T_{NAT}) and ice PSC (T_{ICE}) calculated by assuming 6 ppbv HNO_3 and 4.5 ppmv H_2O are also shown in the figures. The dates when PSCs were observed at Syowa Station identified by the nearest CALIOP data of that day were indicated by asterisks on the bottom of the figures. Over Syowa Station, PSCs were often observed at 15-25 km from the beginning of July (day 183) to the middle of September (day 253) in 2007, and from late June (day 175) to early September (day 251) in 2011.

PSCs were observed only at 18 km after August, due to the sedimentation of PSCs and downwelling of vortex air in late winter as is seen in Figure 3. Although temperatures above Syowa Station were sometimes below T_{NAT} in June and in late September, no PSC was observed during those periods. This may be due to other reasons, such as a different time history of temperature for PSC formation, and/or low HNO_3 (denitrification) and/or H_2O concentration (dehydration) which are needed for PSC formation in late winter season (Saitoh et al., 2006).

Figures 4-7 show time series of HCl, $ClONO_2$, ClO, Cl_y*, O_3, and HNO_3 over Syowa Station in 2007 and 2011 at altitudes of 18 and 22 km for all ground-based and satellite based observations used in this study, respectively. O_3 (sonde) is observed with the KC96 ozonesonde for 2007 and the ECC-1Z ozonesonde for 2011 by JMA. HCl and HNO_3 observed by Aura/MLS are plotted to complement the data lack of FTIR measurements. $ClONO_2$ observed by Envisat/MIPAS is also plotted in the figure. Total inorganic chlorine Cl_y* corresponds to the sum of HCl, $ClONO_2$, and Cl_x, where active chlorine species Cl_x is

defined as the sum of ClO, Cl, and 2*Cl_2O_2 (Bonne et al., 2000). Inferred total inorganic chlorine Cl_y* is calculated from N_2O value (in ppbv) measured by MLS using the polynomial equation derived from the correlation of Cl_y and N_2O (Bonne et al., 2000):

$$Cl_y^*(\text{pptv}) = 4.7070*10^{-7}(N_2O)^4 - 3.2708*10^{-4}(N_2O)^3 + 4.0818*10^{-2}(N_2O)^2 - 4.6856(N_2O) + 3225. \quad (2)$$

The dark shaded area, the light shaded area, and the white area indicate the days when Syowa Station was located outside, in the boundary region, and inside the polar vortex, respectively. Inner and outer edges of the polar vortex were determined as follows:

1) Equivalent latitudes (McIntyre and Palmer, 1984; Butchart and Remsberg, 1986) were computed based on isentropic potential vorticity at 450 K and 560 K isentropic surfaces for 18 km and 22 km using the ERA-Interim reanalysis data (Dee et al., 2011), respectively.

2) Inner and outer edges (at least 5º apart from each other) of the polar vortex were defined by local maxima of the isentropic potential vorticity gradient with respect to equivalent latitude only when a tangential wind speed (i.e., mean horizontal wind speed along the isentropic potential vorticity contour; see Eq. (1) of Tomikawa and Sato (2003)) near the vortex edge exceeds a threshold value (i.e., 20 m s^{-1}, see Nash et al. (1996) and Tomikawa et al. (2015)).

3) Then, the polar region is divided into three regions; i.e., inside the polar vortex (inside of inner edge), the boundary region (between inner and outer edges), and outside the polar vortex (outside of outer edge).

Note that the Syowa Station is often located near the vortex edge and the temporal variations of chemical species observed over Syowa Station reflect the spatial distributions as well as local chemical evolution. The lack of data for ClO and HCl (MLS) from day 195 to day 219, 2007 and $ClONO_2$ from day 170 to day 216, 2007 (upper panels of Figures 4(a) and 6(a)) is due to large error in Aura/MLS or Envisat/MIPAS measurements during this period.

The altitude of 18 km was selected because it was one of the altitudes where nearly complete ozone loss was occurred. The altitude of 22 km, where only about half of the ozone was depleted, was selected to show the difference in the behavior of chemical species from that at 18 km.

The general features of the chemical species observed inside the polar vortex at 18 and 22 km in 2007 and 2011 are summarized as follows: HCl and $ClONO_2$ decreased first, then ClO started to increase in winter, while HCl increases and ClO decreases were synchronized in spring. HCl was almost zero from late June to early September and the day-to-day variations were small over this period (HCl over Syowa Station indicates relatively larger values when it was located at the polar vortex boundary or outside the polar vortex: For example, early August and the beginning of September at 22 km, 2007 in Figure 6). HNO_3 showed large decreases from June to July, and then gradually increased in summer. Day-to-day variations of HNO_3 from June to August were large. O_3 decreased from July to late September when ClO concentration was increased. ClO was enhanced in August and September and the day-to-day variations were large over this period. Cl_y* gradually increased in the polar vortex from late autumn to spring. The Cl_y* value became larger compared with its mixing ratio outside of the polar vortex in spring.

The following characteristics are evident at 18 km (Figures 4 and 5). O_3 gradually decreased from values of 2.5-3 ppmv before winter to values less than one fifth, 0.3-0.5 ppmv, in October. The values of HCl from late June to early September were as small as 0-0.3 ppbv. The recovered values of HCl inside the vortex in spring (October-December) were larger than those before winter and those outside the polar vortex during the same period. $ClONO_2$ inside the vortex kept near zero even after ClO disappeared and did not recover to the level before winter until spring.

At 22 km (Figures 6 and 7), O_3 gradually decreased from winter to spring, but the magnitude of the decrease was much smaller than that at 18 km. The values of HCl from late June to early September were 0-1 ppbv, larger than those at 18 km. The recovered values of HCl in spring were nearly the same as those before winter (around 2.2 ppbv). $ClONO_2$ recovered to larger values than those before winter after ClO disappeared.

As for the temporal increase of $ClONO_2$ in spring during the ClO decreasing phase, we can see a peak of 1.5 ppbv at 18 km in 2011, and at 22 km in both 2007 and 2011 around September 27 (day 270), but we see no temporal increase of $ClONO_2$ at 18 km in 2007.

Figure 7 shows that temporal ClO enhancement and decrease of O_3, $ClONO_2$, and HNO_3 occurred in early winter (May 30-June 19; day 150-170) at 22 km in 2011. This small ozone depletion event before winter may be due to an airmass movement from the polar night area to a sunlit area at lower latitudes. Table 4 summarized the characteristics of variation of minor atmospheric species for 2007 and 2011 at altitudes of 18 and 22 km.

4.2 Time series of ratios of chlorine species

In order to discuss the temporal variations of the chlorine partitioning, the ratios of observed HCl, $ClONO_2$, ClO, and Cl_y with respect to Cl_y* were calculated. Hereafter, we will discuss the ratios of chlorine species only for the cases when Syowa Station was located inside the polar vortex. Here, observed Cl_y is determined as:

$$Cl_y\ (FTIR) = HCl\ (FTIR) + ClONO_2\ (MIPAS) + ClO\ (MLS) \quad (3)$$

$$Cl_y\ (MLS) = HCl\ (MLS) + ClONO_2\ (MIPAS) + ClO\ (MLS). \quad (4)$$

Figures 8 and 9 show the time series of the ratios of each chlorine species with respect to Cl_y* in 2007 (a) and in 2011 (b) at 18 km and 22 km, respectively. For both in 2007 and 2011 at 18 km (Figure 8), the ratio of HCl was 0.6-0.8 and the ratio of $ClONO_2$ was 0.2-0.3 before winter (May 10-20; day 130-140). The partitioning of HCl was three times larger than that of $ClONO_2$ at that time. The ratio of ClO increased to 0.5-0.6 during the ClO enhanced period (the period when ClO values were more than 80 % of its maximum value. See Table 4). The ratio of HCl was 0-0.2 and the ratio of $ClONO_2$ was 0-0.6 during this same period. $ClONO_2$ shows negative correlation with ClO, while HCl kept low even when ClO was low during this period. This negative correlation is shown in Figure 10 later. When ClO was enhanced, the O_3 amount gradually decreased, and finally reached <0.5 ppmv (>80% destruction) in October (October 7; day 280) (See Figures 4 and 5). The ratios became 0.9-1.0 for HCl and 0-0.1 for $ClONO_2$ after the recovery in spring (after October 17; day 290), indicating that almost all chlorine reservoir species became HCl via reaction (R13), due to the lack of O_3 and NO_2 during this period. The ratios of Cl_y (FTIR) and Cl_y (MLS) were both around 0.7 at the time of ClO enhanced period (August 18-September 17; day 230-260). The

remaining chlorine is thought to be Cl_2O_2, which will be shown in model simulation result in Section 4.6. The ratio of Cl_y became close to 1 after the recovery period (after October 7; day 280).

For both in 2007 and 2011 at 22 km (Figure 9), the ratio of HCl was 0.4-0.9 and the ratio of $ClONO_2$ was 0.2-0.3 before winter (April 20-May 20; day 110-140). The partitioning of HCl was two to three times larger than that of $ClONO_2$. The ratio of ClO increased to 0.6-0.7 during the ClO enhanced period (August 8-28; day 220-240 in 2007, August 18-September 7; day 230-250 in 2011). The ratio of HCl was 0-0.3 and the ratio of $ClONO_2$ was 0-0.6 during this period. $ClONO_2$ shows negative correlation with ClO, while HCl kept low even when ClO was low during this period as in the case at 18 km. The O_3 amount gradually decreased during the ClO enhanced period but kept the concentration more than 1.5 ppmv (less than half destruction) at this altitude (See Figures 6 and 7). When the ClO enhancement ended, temporal increase of $ClONO_2$ up to a ratio of 0.5 occurred in early spring (September 17-October 7; day 260-280). Then, the reservoir ratios became 0.6-0.8 for HCl and 0.2-0.4 for $ClONO_2$ in spring (October 7; after day 280). This phenomenon shows that more chlorine deactivation via reaction (R12) occurred towards $ClONO_2$ at 22 km rather than at 18 km. This is attributed to the existence of O_3 and NO_2 during this period at 22 km, which was different from the case at 18 km. The ratios of Cl_y (FTIR) and Cl_y (MLS) were both around 0.8 at the time of ClO enhanced period (August 8-28; day 220-240 in 2007, August 18-September 7; day 230-250 in 2011). The remaining chlorine is thought to be Cl_2O_2. The ratio of Cl_y became around 1.1 after the recovery period (after September 27; day 270). The reason why observed Cl_y values exceed calculated Cl_y* values might be because the N_2O-Cl_y correlation from the one in the equation (2) is not applicable at this altitude.

In 2011 at 18 km (Figure 8), another temporal increase of $ClONO_2$ up to a ratio of 0.6 occurred in early spring (around October 7; day 280) in accordance with HCl increase, then the $ClONO_2$ amount gradually decreased to nearly zero after late October (after October 27; day 300). This temporal increase in $ClONO_2$ could be attributed to temporal change of the location of Syowa Station in the polar vortex. Although Syowa Station was judged to be inside the polar vortex during July 14-December 16 (day 195-350) by our analysis, the difference between the equivalent latitude over Syowa Station and that at inner edge became less than 10 degrees at around October 7 (day 280), while it was typically between 15 and 20 degrees in other days. O_3 and HNO_3 showed higher values around October 7 (day 280) (see Figure 5), indicating that Syowa Station was located close to the boundary region at this period. Therefore, the temporal increase of $ClONO_2$ in 2011 at 18 km was attributed to spatial variation, not to chemical evolution.

4.3 Correlation between ClO and $ClONO_2$

Figure 10 shows the correlation between ClO and $ClONO_2$ during the ClO enhanced period (August 8-September 17; day 220-260) at 18 km in 2007 (a) and 2011 (b), and at 22 km in 2007 (c) and 2011 (d). In this plot, the location of Syowa Station with respect to the polar vortex (inside, the boundary region, and outside the polar vortex) is indicated by different symbols. Note that MLS ClO and MIPAS $ClONO_2$ data were sampled on the same day at the nearest orbit to Syowa Station for both satellites. The maximum differences between these two satellites' observational times and locations are 9.0 hours in time and 587 km in distance. Mean differences are 6.8 hours in time and 270 km in distance, respectively. Solid lines show regression

lines obtained by RMA (Reduced Major Axis) regression. Negative correlations of slope about -1.0 between ClO and $ClONO_2$ are seen in all figures. The cause of this negative correlation might be due to the variation of the relative distance between Syowa Station and the boundary region of the polar vortex. When Syowa Station was located deep inside the polar vortex, there was more ClO and less $ClONO_2$. On the contrary when Syowa Station was located near the vortex edge, there was less ClO and more $ClONO_2$. The equivalent latitude over Syowa Station shown by color code generally show this tendency, that warm coloured higher equivalent latitude points are located more towards the bottom right-hand side. This is further confirmed by 3-dimensional model simulation as shown later.

4.4 Comparison with model results

Figures 11 and 12 show comparisons of daily time series of simulated mixing ratios of ClO, HCl, $ClONO_2$, Cl_y, and O_3 by the MIROC3.2 Chemistry-Climate Model (CCM) (Akiyoshi et al., 2016) with FTIR, Aura/MLS, and Envisat/MIPAS measurements at 18 km and 22 km, respectively. For a description of the MIROC3.2 CCM, please see Appendix for detail. In these figures, Cl_y for Aura/MLS in the panels (d) and (i) actually represents the Cl_y* value calculated by equation (2) using the N_2O value measured by Aura/MLS. Cl_y from the MIROC3.2 CCM is the sum of total reactive chlorines, i.e., $Cl_y = Cl + 2*Cl_2 + ClO + 2*Cl_2O_2 + OClO + HCl + HOCl + ClONO_2 + ClNO_2 + BrCl$. Note that we plotted modeled values at 12h UTC (~15h local time of Syowa Station) calculated by the MIROC3.2 CCM in order to compare the daytime measurements of FTIR and satellites. In Figures 11(b), (d), (g), and (i), modeled HCl and Cl_y showed systematically smaller values compared with FTIR or MLS measurements. The cause of this discrepancy may be partly due to either smaller downward advection and/or faster horizontal mixing of airmass across the subtropical barrier in MIROC3.2 CCM (Akiyoshi et al., 2016). Another possibility of the discrepancy is the difference of Cl_y*-N_2O correlation used to calculate the Cl_y* value by equation (2), since this correlation comes from the aircraft measurement in summer (Bonne et al., 2000). Nevertheless, evolutions of measured HCl and $ClONO_2$ for the period are well simulated by the MIROC3.2 CCM. Modeled O_3 were in very good agreement with FTIR and/or MLS measurements throughout the year in both altitudes for both years. Hereafter, the result of MIROC3.2 CCM at 50 hPa (~18 km) is discussed.

4.5 Polar distribution of minor species

Figure 13 shows distribution of simulated mixing ratios of O_3, NO_2, HNO_3, ClO, HCl, and $ClONO_2$ by the MIROC3.2 CCM at 50 hPa for June 24 (day 175), September 2 (day 245), September 6 (day 249), and October 6 (day 279) in 2007. Polar vortex boundary defined by the maximum gradient of potential vorticity at 475 K calculated from ERA-Interim reanalysis data was plotted by dotted circle. This boundary was located in between the inner and the outer edges of the polar vortex as were defined in Section 4.1. The location of Syowa Station is shown by a white star in each panel. On June 24 (day 175), stratospheric temperatures over Antarctica were already low enough to allow PSCs to form. Consequently, NO_2 and HNO_3 in the polar vortex condensed onto PSCs. Note that the depleted area of NO_2 was greater than that of HNO_3. This is due to reaction (R12) that converts ClO and NO_2 to $ClONO_2$ at the edge of the polar vortex, which is shown by the enhanced $ClONO_2$

area at the vortex edge in Figure 13. Also, HCl and $ClONO_2$ are depleted in the polar vortex due to the heterogeneous reactions (R1), (R2), (R3), and (R4) on the surface of PSCs and aerosols. Some HCl remains near the core of the polar vortex, because the initial amount of the counter-part of heterogeneous reaction (R1) ($ClONO_2$) was less than that of HCl. The O_3 amount was only slightly depleted within the polar vortex on this day.

On September 2 (day 245), amounts of NO_2, HNO_3, HCl, and $ClONO_2$ all show very depleted values in the polar vortex. The amount of ClO shows some enhanced values at the outer part of the polar vortex. Development of ozone depletion was seen in the polar vortex. Note that $ClONO_2$ shows enhanced values around the boundary region of the polar vortex. This might be due to the reaction (R12) at this location. On this day (day 245), Syowa Station was located inside the polar vortex close to the inner vortex edge, where ClO was smaller and $ClONO_2$ was greater than the values deep inside the polar vortex as observed and indicated by upper left circle with cross in Figure 10 (a).

On September 6 (day 249), most features were the same as on September 2, but the shape of the polar vortex was different. Consequently, Syowa Station was located deep inside the polar vortex, where ClO was greater and $ClONO_2$ was smaller than the values around the boundary region of the polar vortex as observed and indicated by lower right circle with cross in Figure 10 (a). Hence, the negative correlation between ClO and $ClONO_2$ seen in Figure 10 was due to variation of the relative distance between Syowa Station and the inner edge of the polar vortex.

As for HCl, it kept nearly zero value not only on this day (September 6) but also on September 2 when Syowa Station was located inside the polar vortex close to the inner vortex edge. Therefore, observed day-to-day variations of HCl were small and did not show any correlation with ClO (see Figures 4-7).

On October 6 (day 279), ClO enhancement has almost disappeared. Inside the polar vortex, O_3, NO_2, HNO_3, and $ClONO_2$ showed very low values. Ozone was almost fully destroyed at this altitude in the polar vortex. However, the amount of HCl increased deep inside the polar vortex. This might be due to the recovery of HCl by reaction (R13) deep inside the polar vortex, where there was no O_3 or NO_2 left and reaction (R13) was favoured compared with reaction (R12). Syowa Station was located deep inside the polar vortex and the simulated and observed amounts of HCl were both more than ten times greater than those of $ClONO_2$ on this day (see Figure 4).

Figure 14 shows the distribution of simulated mixing ratios of O_3, NO_2, HNO_3, ClO, HCl, and $ClONO_2$ by the MIROC3.2 CCM at 50 hPa for July 5 (day 186), August 19 (day 231), August 21 (day 233), and October 9 (day 282) in 2011. Polar vortex boundary and location of Syowa Station were also plotted. On July 5 (day 186), the situation was similar to that of June 24 (day175) in 2007. Syowa Station was located deeper inside the polar vortex on July 5 in 2011 than on June 24 in 2007 and remaining HCl was observed by MLS (see Figure 5).

On August 19 (day 231) and August 21 (day 233), the situations were similar to those of September 2 (day 245) and September 6 (day 249) in 2007, respectively. ClO and $ClONO_2$ correlations on these days are also indicated by circles with crosses in Figure 10 (b).

On October 9 (day 282), the situation was similar to that of October 6 (day 279) in 2007, but Syowa Station was located inside the polar vortex closer to the inner vortex edge than in 2007. The recovery of $ClONO_2$ by reaction (R12) was simulated

and observed at Syowa Station besides the recovery of HCl by reaction (R13), because there were some O_3 and NO_2 near the inner vortex edge (see Figure 5). This shows the phenomena described on the last paragraph in Section 4.2.

4.6 Time evolution of chlorine species from CCM

Three-hourly time series of zonal-mean active chlorine species, Cl_2O_2 (b), Cl_2 (c), ClO (d), and their sum ($ClO+2*Cl_2O_2+2*Cl_2$) (a), and chlorine reservoir species HCl (e) and $ClONO_2$ (f) modeled by MIROC3.2 CCM at 68.4ºS, 71.2ºS, 76.7ºS, and 87.9ºS in 2007 are plotted in Figure 15. The dates on which the distribution of each species is shown in Figure 13 are indicated by vertical dotted lines. In Figure 15, it is shown that HCl and $ClONO_2$ rapidly decreased at around May 10 (day 130) at 87.9ºS, when PSCs started to form in the Antarctic polar vortex (Figures 15(e) and 15(f)). The decrease of HCl stopped when the counter-part of the heterogeneous reaction (R1) ($ClONO_2$) was missing at around May 20 (day 140). Consequently, Cl_2 was formed (Figure 15(c)). Similar chlorine activation was seen at 76.7ºS about 5-10 days later than at 87.9ºS. Gradual conversion from Cl_2 into Cl_2O_2 (ClO-dimer) was seen at all latitudes at around May 30-June 9 (day 150-160) (Figures 15(b) and 15(c)) through reactions (R5), (R8), and (R9). At 87.9ºS, conversion from Cl_2 to Cl_2O_2 was slow, due to lack of sunlight which is needed for reaction (R5). Increase of ClO occurred much later in winter (July 9; day 190 or later), because sun light is needed to form ClO by reactions (R5) and (R8) in the polar vortex (Figure 15(d)). Nevertheless, there were some enhancements of ClO in early winter, June 24 (day 175), simulated at the edge of the polar vortex (Figure 13) where there was some sunlight available due to the distortion of the shape of the polar vortex. Increase of ClO occurred from lower latitude (68.4ºS) at around July 14 (day 195), towards higher latitude (87.9ºS) at around August 13 (day 255) (Figure 15(d)). Diurnal variation of ClO was also seen at latitudes between 68.4ºS and 76.7ºS. When the stratospheric temperature increased above PSC saturation temperature at around September 27 (day 270) (Figure 3(a)), chlorine activation ended, and ClO was mainly converted into HCl at all latitudes inside the polar vortex (Figures 15(d) and 15(e)). This is because reaction (R13) occurs more frequently than reaction (R12) inside the polar vortex due to the depleted O_3 amount there as was described in Section 1 (Douglass et al., 1995).

Continuous loss of HCl was seen at 87.9ºS between June 9 (day 160) and July 19 (day 200) even after the disappearance of the counterpart of heterogeneous reaction (R1) (Figure 15(e)). The cause of this continuous loss was unknown until recently, where a hypothesis was proposed that includes the effect of decomposition of particulate HNO_3 by some process like ionisation caused by galactic cosmic rays during the winter polar vortex (Grooß et al., 2018). Solomon et al. (2015) proposed a new mechanism on this issue: Continuous transport of $ClONO_2$ from the subpolar regions near 55-65ºS to higher latitudes near 65-75ºS provides a flux of NO_x from more sunlit latitudes into the polar vortex. Our result is consistent with the mechanism proposed by Solomon et al. (2015), which was indicated by some sporadic increase in $ClONO_2$ at around June 7 (day 158), June 28 (day 179), and July 8 (day 189) at 76.7ºS as shown in Figure 15(f). Subsequently, HCl losses were observed at 76.7ºS and 87.9ºS during these episodes in Figure 15(e). Thus, the continuous loss of HCl at the most polar latitude (87.9ºS) can be due to the gradual mixing of air within the polar vortex during the winter period, when polar vortex was still strong.

5. Conclusions

Lower stratospheric vertical profiles of O_3, HNO_3, and HCl were retrieved using SFIT2 from solar spectra taken with a ground-based FTIR installed at Syowa Station, Antarctica from March to December 2007 and September to November 2011. This was the first continuous measurements of chlorine species throughout the ozone hole period from the ground in Antarctica. Retrieved profiles were validated with Aura/MLS and ozonesonde data. The absolute differences between FTIR and Aura/MLS or ozonesonde measurements were within measurement error bars at the altitudes of interest.

To study the temporal variation of chlorine partitioning and ozone destruction from fall to spring in the Antarctic polar vortex, we analyzed temporal variations of measured minor species by FTIR over Syowa Station combined with satellite measurements of ClO, HCl, $ClONO_2$ and HNO_3. When the stratospheric temperature over Syowa Station fell well below NAT PSC saturation temperature, PSCs started to form and heterogeneous reaction between HCl and $ClONO_2$ occurred and $ClONO_2$ was almost completely depleted at both 18 km and 22 km in early winter. When the sun came back to the Antarctic in spring, enhancement of ClO and gradual O_3 destruction were observed. During the ClO enhanced period, negative correlation between ClO and $ClONO_2$ was observed in the time-series of the data at Syowa Station. This negative correlation is associated with the distance between Syowa Station and the inner edge of the polar vortex.

To see the comprehensive behavior of chlorine and related species inside the polar vortex and the boundary region in more detail, results of MIROC3.2 CCM simulation were analyzed. Direct comparison between CCM results and observations show good day-to-day agreement in general, although some species show systematic differences especially at 18 km. The modeled O_3 is in good agreement with FTIR and satellite observations. Rapid conversion of chlorine reservoir species (HCl and $ClONO_2$) into Cl_2, gradual conversion of Cl_2 into Cl_2O_2, increase of ClO when sunlight became available, and conversion of ClO into HCl were successfully reproduced by the CCM. HCl decrease in the winter polar vortex core continued to occur due to the transport of $ClONO_2$ from the subpolar region to higher latitudes, providing a flux of $ClONO_2$ from more sunlit latitudes into the polar vortex. Temporal variation of chlorine species over Syowa Station was affected both by heterogeneous chemistry related to PSC occurrence deep inside the polar vortex, and transport of NO_x-rich airmass from lower latitudinal polar vortex boundary region, which can produce additional $ClONO_2$ by reaction (R12).

The deactivation pathways from active ClO into reservoir species (HCl and/or $ClONO_2$) were found to be very dependent on the availability of ambient O_3. At an altitude (18 km) where most ozone was depleted in the Antarctic, most ClO was converted to HCl. However, at an altitude (22 km) when there was some O_3 available, additional increase of $ClONO_2$ than pre-winter value can occur, as in the case in the Arctic, through reactions (R15) and (R12) (Douglass et al., 1995; Grooß et al., 1997).

Appendix: MIROC3.2 nudged chemistry–climate model

The chemistry-climate model (CCM) used in this study was MIROC3.2 CCM, which was developed on the basis of version 3.2 of the Model for Interdisciplinary Research on Climate (MIROC3.2) general circulation model (GCM). The MIROC3.2 CCM introduces the stratospheric chemistry module of the old version of the CCM that was used for simulations proposed by the chemistry–climate model validation (CCMVal) and the second round of CCMVal (CCMVal2) (WMO, 2007, 2011; SPARC CCMVal, 2010; Akiyoshi et al., 2009, 2010). The MIROC3.2 CCM is a spectral model with a T42 horizontal resolution (2.8° × 2.8°) and 34 vertical atmospheric layers above the surface. The top layer is located at approximately 80 km (0.01 hPa). Hybrid sigma–pressure coordinates are used for the vertical coordinate. The horizontal wind velocity and temperature in the CCM were nudged toward the ERA–Interim data (Dee et al., 2011) to simulate global distributions of ozone and other chemical constituents on a daily basis. The transport is calculated by a semi–Lagrangian scheme (Lin and Rood, 1996). The chemical constituents included in this model are O_x, HO_x, NO_x, ClO_x, BrO_x, hydrocarbons for methane oxidation, heterogeneous reactions for sulfuric-acid aerosols, supercooled ternary solutions, nitric-acid trihydrate, and ice particles. The CCM contains 13 heterogeneous reactions on multiple aerosol types as well as gas-phase chemical reactions and photolysis reactions. The reaction-rate and absorption coefficients are based on JPL–2010 (Sander et al., 2010). See Akiyoshi et al. (2016) for more details.

Acknowledgments

We acknowledge all the members of the 48th Japanese Antarctic Research Expedition (JARE-48), JARE-52 for their support in making the FTIR observation at Syowa Station. Data provision of Aura/MLS and Envisat/MIPAS are much appreciated. We thank Japan Meteorological Agency for providing the ozonesonde and Rawin sonde data at Syowa Station. Thanks are due to Dr. Yosuke Yamashita for performing the CCM run and Dr. Eric Dupuy for preparing figures of the model output. The model computations were performed on NEC-SX9/A(ECO) and NEC SX-ACE computers at the CGER, NIES, supported by the Environment Research and Technology Development Funds of the Ministry of the Environment (2-1303) and Environment Restoration and Conservation Agency (2-1709). We thank Dr. Takafumi Sugita for useful discussion and comments.

References

Anderson, J., Russell, J. M., III, Solomon, S., and Deaver, L. E.: Halogen Occultation Experiment confirmation of stratospheric chlorine decreases in accordance with the Montreal Protocol, J. Geophys. Res., 105, 4483-4490, doi:10.1029/1999jd901075, 2000.

Akiyoshi, H., Zhou, L. B., Yamashita, Y., Sakamoto, K., Yoshiki, M., Nagashima, T., Takahashi, M., Kurokawa, J., Takigawa, M., and Imamura, T.: A CCM simulation of the breakup of the Antarctic polar vortex in the years 1980–2004 under the CCMVal scenarios, J. Geophys. Res., 114, D03103(1–28), doi:10.1029/2007JD009261, 2009.

Akiyoshi, H., Y. Yamashita, K. Sakamoto, L. B. Zhou, and T. Imamura: Recovery of stratospheric ozone in calculations by the Center for Climate System Research/National Institute for Environmental Studies chemistry–climate model under the CCMVal–REF2 scenario and a no–climate–change run, J. Geophys. Res., 115, D19301(1–22), doi:10.1029/2009JD012683, 2010.

Akiyoshi, H., Nakamura, T., Miyasaka, T., Shiotani, M., and Suzuki, M.: A nudged chemistry-climate model simulation of chemical constituent distribution at northern high-latitude stratosphere observed by SMILES and MLS during the 2009/2010 stratospheric sudden warming, J. Geophys. Res. Atmos., 121, 1361-1380, doi:10.1002/2015JD023334, 2016.

Anderson, J. G., Brune, W. H., and Proffitt, M. H.: Ozone destruction by chlorine radicals within the Antarctic vortex: The spatial and temporal evolution of ClO-O_3 anticorrelation based on in situ ER-2 data, J. Geophys. Res., 94, 11,465-11479, 1989.

Anderson, J., Russell, J. M., III, Solomon, S., and Deaver, L. E.: Halogen Occultation Experiment confirmation of stratospheric chlorine decreases in accordance with the Montreal Protocol, J. Geophys. Res., 105, 4483-4490, doi:10.1029/1999jd901075, 2000.

Blumenstock, T., Kopp, G., Hase, F., Hochschild, G., Mikuteit, S., Raffalski, U., and Ruhnke, R.: Observation of unusual chlorine activation by ground-based infrared and microwave spectroscopy in the late Arctic winter 2000/01, Atmos. Chem. Phys., 6, 897-905, 2006.

Bonne, G. P., Stimpf1le, R. M., Cohen, R. C., Voss, P. B., Perkins, K. K., Anderson, J. G., Salawitch, R. J., Elkins, J. W., Dutton, G. S., Jucks, K. W., and Toon, G. C.: An examination of the inorganic chlorine budget in the lower stratosphere, J. Geophys..Res., 105, D2, 1957-1971, 2000.

Butchart, N., and Remsberg, E. E.: The area of the stratospheric polar vortex as a diagnostic for tracer transport on an isentropic surface, J. Atmos. Sci., 43, 1319–1339, 1986.

Canty, T. P., Salawitch, R. J., and Wilmouth, D. M.: The kinetics of the ClOOCl catalytic cycle, J. Geophys. Res., 121, 13,768-13, 783, doi:10.1002/2016JD025710, 2016.

Chubachi, S.: Preliminary result of ozone observation at Syowa Station from February 1982 to January 1983, Mem. Natl Inst. Polar Res., Spec. Issue, 34, 13-19, 1984.

Connor, B., Parrish, A., Tsou, J., and McCormick, M.: Error analysis for the ground-based microwave ozone measurements during STOIC, J. Geophys. Res., 100, 9283-9291, 1995.

de Laat, A. T. J., van Weele, M., and van der A, R. J.: Onset of stratospheric ozone recovery in the Antarctic ozone hole in assimilated daily total ozone columns, J. Geophys. Res., 122, 11,880-11,899, doi:10.1002/2016JD025723, 2017.

Dee, D. P., Uppala, S. M., Simmons, A. J., Berrisford, P., Poli, P., Kobayashi, S., Andrae, U., Balmaseda, M. A., Balsamo, G., Bauer, P., Bechtold, P., Beljaars, A. C. M., van de Berg, L., Bidlot, J., Bormann, N., Delsol, C., Dragani, R., Fuentes, M.,

Geer, A. J., Haimberger, L., Healy, S. B., Hersbach, H., Hólm, E. V., Isaksen, L., Kållberg, P., Köhler, M., Matricardi, M., McNally, A. P., Monge-Sanz, B. M., Morcrette, J. -J., Park, B. -K., Peubey, C., de Rosnay, P., Tavolato, C., Thépaut, J. -N., and Vitart, F.: The ERA–Interim reanalysis: configuration and performance of the data assimilation system, Q. J. R. Meteorol. Soc., 137, 553–597, doi:10.1002/qj.828, 2011.

Douglass, A. R., Schoeberl, M. R., Stolarski, R. S., Waters, J. W., Russell, J. M., III, Roche, A. E., and Massie, S. T.: Interhemispheric differences in springtime production of HCl and $ClONO_2$ in the polar vortices, J. Geophys. Res., 100, 13,967-13,978, 1995.

Drdla, K. and Müller, R.: Temperature thresholds for chlorine activation and ozone loss in the polar stratosphere, Ann. Geophys., 30, 1055-1073, doi:10.5194/angeo-30-1055-2012, 2012

Dufour, G., Nassar, R., Boone, C. D., Skelton, R., Walker, K. A., Bernath, P. F., Rinsland, C. P., Semeniuk, K., Jin, J. J., McConnell, J. C., and Manney, G. L.: Partitioning between the inorganic chlorine reservoirs HCl and $ClONO_2$ during the Arctic winter 2005 from the ACE-FTS, Atmos. Chem. Phys., 6, 2355-2366, 2006.

Farman, J. C., Gardiner, B. G., and Shanklin, J. D.: Large losses of total ozone in Antarctica reveal seasonal ClOx/NOx interaction, Nature, 315, 207-210, 1985.

Farmer, C. B., Toon, G. C., Schaper, P. W., Blavier, J. -F., and Lowes, L. L.: Stratospheic trace gases in the spring 1986 Antarctic atmosphere, Nature, 329, 126-130, 1987.

Fischer, H., and Oelhaf, H.: Remote sensing of vertical profiles of atmospheric trace constituents with MIPAS limb-emission spectrometers, Appl. Opt., 35, 2787-2796, 1996.

Fischer, H., Birk, M., Blom, C., Carli, B., Carlotti, M., von Clarmann, T., Delbouille, L., Dudhia, A., Ehhalt, D., Endemann, M., Flaud, J. M., Gessner, R., Kleinert, A., Koopmann, R., Langen, J., López-Puertas, M., Mosner, P., Nett, H., Oelhaf, H., Perron, G., Remedios, J., Ridolfi, M., Stiller, G., and Zander, R.: MIPAS: An instrument for atmospheric and climate research, Atmos., Chem. Phys., 8, doi:10.5194/acp-8-2151-2008, 2008.

Froidevaux, L., et al.: Early validation analyses of atmospheric profiles from EOS MLS on the Aura satellite, IEEE Trans. Geosci. Remote Sens., 44, 1106-1121, 2006.

Gallery, W. O., Kneizys, F. S., and Clough, S. A.: Air mass computer program for atmospheric transmittance/radiance calculation: FSCATM, Environmental Research Paper ERP-828/AFGL-TR-83-0065, Air Force Geophysical Laboratory, Bedford, MA, USA, 1983.

Grooß, J. -U., Pierce, R. B., Crutzen, P. J., Grose, W. L., and Russell III, J. M.: Reformation of chlorine reservoirs in southern hemisphere polar spring, J. Geophys., Res., 102, 13,141-13,152, doi:10.1029/96JD03505, 1977.

Grooß, J. -U., Brautzsch, K., Pommrich, R., Solomon, S., and Müller, R.: Stratospheric ozone chemistry in the Antarctic: what determines the lowest ozone values reached and their recovery?, Atmos. Chem. Phys., 11, 12,217-12,226, doi:10.5194/acp-11-12217-2011, 2011.

Grooß, J. -U., Müller, R, Spang, R., Tritscher, I., Wegner, T., Chipperfield, M. P., Feng, W., Kinnison, D. E., and Madronich, S.: On the discrepancy of HCl processing in the core of the wintertime polar vortices, Atmos. Chem. Phys., 18, 8647-8666, doi:10.5194/acp-18-8647-2018, 2018

Hase, F, Hannigan, J. W., Co1ey, M. T., Goldman, A., Höpfner, M., Jones, N. B., Rinsland, C. P., Wood, S. W.: Intercomparison of retrieval codes used for the analysis of high-resolution, ground-based FTIR measurements, J. Quant. Spectrosc. Radiat. Transfer, 87, 25-52, 2004.

Hayashida, S., Sugita, T., Ikeda, N., Toda, Y., and Irie, H.: Temporal evolution of $ClONO_2$ observed with Improved Limb Atmospheric Spectrometer (ILAS) during Arctic late winter and early spring in 1997, J. Geophys. Res., 112, D14311, doi:10.1029/2006JD008108, 2007.

Höpfner, M., von Clarmann, T., Fischer, H., Glatthor, N., Grabowski, U., Kellmann, S., Kiefer, M., Linden, A., Mengistu Tsidu, G., Milz, M., Steck, T., Stiller, G. P., Wang, D. Y., and Funke, B.: First spaceborne observations of Antarctic stratospheric $ClONO_2$ recovery: Austral spring 2002, J. Geophys. Res., 109, D11308, doi:10.1029/2004JD004609, 2004.

Höpfner, M., von Clarmann, T., Fischer, H., Funke, B., Glatthor, N., Grabowski, U., Kellmann, S., Kiefer, M., Linden, A., Milz, M., Steck, T., Stiller, G. P., Bernath, P., Blom, C. E., Blumenstock, Th., Boone, C., Chance, K., Coffey, M. T., Friedl-Vallon, F., Griffith, D., Hannigan, J. W., Hase, F., Jones, N., Jucks, K. W., Keim, C., Kleinert, A., Kouker, W., Liu, G. Y., Mahieu, E., Mellqvist, J., Mikuteit, S., Notholt, J., Oelhaf, H., Piesch, C., Reddmann, T., Ruhnke, R., Schneider, M., Strandberg, A., Toon, G., Walker, K. A., Warneke, T., Wetzel, G., Wood, S., and Zander, R.: Validation of MIPAS $ClONO_2$ measurements, Atmos. Chem. Phys., 7, 257-281, 2007.

Ko, M. K. W., Rodriguez, J. M., Sze, N. D., Proffitt, M. H., Starr, W. L., Krueger, A., Browell, E. V., McCormick, M. P.: Implications of AAOE observations for proposed chemical explanations of the seasonal and interannual behavior of Antarctic ozone, J. Geophys..Res., 94, D14, 16,705-16,715, 1989.

Kreher, K., Keys, J. G., Johnston, P. V., Platt, U., and Liu, X.: Ground-based measurements of OClO and HCl in austral spring 1993 at Arrival Heights Antarctica, Geophys. Res. Lett., 23, 1545-1548, 1996.

Kuttippurath, J., Goutail, F., Pommereau, J. -P., Lefèvre, F., Roscoe, H. K., Pazmiño, A., Feng, W., Chipperfield, M. P., and Godin-Beekmann, S.: Estimation of Antarctic ozone loss from ground-based total column measurements, Atmos. Chem. Phys., 10, 6569-6581, 2010.

Lin, S.-J. and Rood, R. B.: Multidimensional flux-form semi-Lagrangian transport schemes, Mon. Wea. Rev., 124, 2046-2070, 1996.

Liversey, N., Van Snyder, W., Read, W., and Wagner, P.: Retrieval algorithms for the EOS Microwave Limb Sounder (MLS), Geoscience and Remote Sensing, IEEE Transactions, 44, 1144-1155, doi:10.1109/TGRS.2006.872327, 2006.

Livesey, N. J., Read, W. G., Wagner, P. A., Froidevaux, L., Lambert, A., Manney, G. L., Millán Valle, L. F., Pumphrey, H. C., Santee, M. L., Schwartz, M. J., Wang, S., Fuller, R. A., Jarnot, R. F., Knosp, B. W., Martinez, E., and Lay, R. R.: Version 4.2x Level 2 data quality and description document, Jet Propul. Lab., Tech. Rep. JPL D-33509 Rev. D, Pasadena, CA, USA (Available from http://mls.jpl.nasa.gov.), 2018.

Manney, G. L., Santee, M. L, Rex, M., Livesey, N. J., Pitts, M. C., Veefkind, P., Nash, E. R., Wohltmann, I., Lehmann, R., Froidevaux, L., Poole, L. R., Schoeberl, M. R., Haffner, D.P., Davies, J., Dorokhov, V., Gernandt, H., Johnson, B., Kivi, R., Kyrö, E., Larsen, N., Levelt, P. F., Makshtas, A., McElroy, C. T., Nakajima, H., Parrondo, M. C., Tarasick, D. W., von der Gathen, P., Walker, K. A., and Zinoviev, N. S.: Unprecedented Arctic ozone loss in 2011, Nature, 478, 469-475, doi:10.1038/nature10556, 2011.

McIntyre, M. E., and Palmer, T. N.: The 'surf zone' in the stratosphere, J. Atmos. Terr. Phys., 46, 825–849, 1984.

Mellqvist, J., Galle, B., Blumenstock, T., Hase, F., Yashcov, D., Notholt, J., Sen, B., Blavier, J. -F., Toon, G. C., and Chipperfield, M. P.: Ground-based FTIR observations of chlorine activation and ozone depletion inside the Arctic vortex during the winter of 1999/2000, J. Geophys.. Res., 107, D20, 8263, doi:10.1029/2001JD001080, 2002.

Michelsen, H. A., Webster, C. R., Manney, G. L., Scott, D. C., Margitan, J. J., May, R. D., Irion, F. W., Gunson, M. R., Russell III, J. M., and Spivakovssky, C. M.: Maintenance of high HCl/Cl_y and NO_x/NO_y in the Antarctic vortex: A chemical signature of confinement during spring, J. Geophys.. Res., 104, 26,419-26,436, 1999.

Müller, R., Peter, T., Crutzen, P. J., Oelhaf, H., Adrian, G. P., v. Clarmann, T., Wegner, A., Schmidt, U., and Lary, D.: Chlorine chemistry and the potential for ozone depletion in the Arctic stratosphere in the winter of 1991/92, Geophys. Res. Lett., 21, 1427-1430, 1994.

Müller, R., Crutzen, P. J., Grooß, J. -U., Brühl, C., Russell III, J. M., and Tuck, A. F.: Chlorine activation and ozone depletion in the Arctic vortex:Observations by the Halogen Occultation Experiment on the Upper Atmosphere Research Satellite, J. Geophys. Res., 101, D7, 12,531-12,554, 1996.

Nakajima, H.: Preface to special section on ILAS-II: The Improved Limb Atmospheric Spectrometer II, J. Geophys. Res., 111, D20S90, doi:10.1029/2006jd007412, 2006.

Nakajima, H., Sugita, T., Yokota, T., Ishigaki, T., Mogi, Y, Araki, N, Waragai, K, Kimura, N, Iwazawa, T., Kuze, A, Tanii, J, Kawasaki, H, Horikawa, M, Togami, T, Uemura, N, Kobayashi, H, and Sasano, Y.: Characteristics and performance of the Improved Limb Atmospheric Spectrometer-II (ILAS-II) on board the ADEOS-II satellite, J. Geophys. Res., 111, D11S01, doi:10.1029/2005JD006334, 2006.

Nakajima, H., Wohltmann, I, Wegner, T., Takeda, M., Pitts, M. C., Poole, L. R., Lehmann, R., Santee, M. L., and Rex, M.: Polar stratospheric cloud evolution and chlorine activation measured by CALIPSO and MLS, and modeled by ATLAS, Atmos. Chem. Phys., 16, 3311-3325, doi:10.5194/acp-16-3311-2016, 2016.

Nash, E. R., Newman, P. A., Rosenfield, J. E., and Schoeberl, M. R.: An objective determination of the polar vortex using Ertel's potential vorticity, J. Geophys. Res., 101, 9471–9478, 1996.

Norton, R., and Rinsland, C.: ATMOS data processing and science analysis methods, Appl. Opt., 30, 389-400, 1991.

Oelhaf, H., v. Clarmann, T., Fischer, H., Friedl-Vallon, F., Fritzsche, C., Linden, A., Piesch, C. Seefeldner, M., and Völker, W.: Stratospheric $ClONO_2$ and HNO_3 profiles inside the Arctic vortex from MIPAS-B limb emission spectra obtained during EASOE, Geophys. Res. Lett., 21, 1263-1266, doi:10.1029/93GL01303, 1994.

Parrish, A., Connor, B., Tsou, J., McDermid, I., and Chu, W.: Ground-based microwave monitoring of stratospheric ozone, J. Geophys. Res., 97, 2541-2546, 1992.

Pitts, M. C., Thomason, L. W., Poole, L. R., and Winker, D. M.: Characterization of Polar Stratospheric Clouds with spaceborne lidar: CALIPSO and the 2006 Antarctic season, Atmos. Chem. Phys., 7, 5207-5228, doi:10.5194/acp-7-5207-2007, 2007.

Pitts, M. C., Poole, L. R., and Thomason, L. W.: CALIPSO polar stratospheric cloud observations: second-generation detection algorithm and composition discrimination, Atmos. Chem. Phys., 9, 7577-7589, doi:10.5194/acp-9-7577-2009, 2009.

Pitts, M. C., Poole, L. R., Dörnbrack, A., and Thomason, L.W.: The 2009–2010 Arctic polar stratospheric cloud season: a CALIPSO perspective, Atmos. Chem. Phys., 11, 2161–2177, doi:10.5194/acp-11-2161-2011, 2011.

Rees, D., Barnett, J. J., and Labitske, K.: COSPAR International Reference Atmosphere: 1986, Part II, Middle Atmosphere Models, Adv. Space Res., 10, 1-525, 1990.

Rinsland, C. P., Jones, N. B., Connor, B. J., Logan, J. A., Pougatchev, N. S., Goldman, A., Murcray, F. J., Stephen, T. M., Pine, A. S., Zander, R., Mahieu, E., and Demoulin, P.: Northern and Southern Hemisphere ground-based infrared spectroscopic measurements of tropospheric carbon monoxide and ethane, J. Geophys. Res., 103, 28,197-28,218, 1998.

Rodgers, C. D.: Inverse methods for atmospheric sounding: Theory and practice., World Scientific, Singapore, 2000.

Saitoh, N., Hayashida, S., Sugita, T., Nakajima, H., Yokota, T., Hayashi, M., Shiraishi, K., Kanzawa, H., Ejiri, M. K., Irie, H., Tanaka, T., Terao, Y., Bevilacqua, R. M., Randall, C. E., Thomason, L. W., Taha, G., Kobayashi, H., and Sasano, Y.: Intercomparison of ILAS-II version 1.4 aerosol extinction coefficient at 780 nm with SAGE II, SAGE III, and POAM III, J. Geophys. Res., 111, D11S05, doi:10.1029/2005JD006315, 2006.

Sander, S. P., Abbatt, J., Barker, J. R., Burkholder, J. B., Friedl, R. R., Golden, D. M., Huie, R. E., Kolb, C. E., Kurylo, M. J., Moortgat, G. K., Orkin, V. L. and Wine, P. H.: Chemical Kinetics and Photochemical Data for Use in Atmospheric Studies, Evaluation No. 17, JPL Publication 10-6, Jet Propulsion Laboratory, Pasadena, http://jpldataeval.jpl.nasa.gov/, 2011.

Santee, M. L., Manney, G. L., Waters, J. W., and Livesey, N. J.: Variations and climatology of ClO in the polar lower stratosphere from UARS Microwave Limb Sounder measurements, J. Geophys.. Res., 108, D15, 4454, doi:10.1029/2002JD003335, 2003.

Santee, M. L., MacKenzie, I. A., Manney, G. L., Chipperfield, M. P., Bernath, P. F., Walker, K. A., Boone, C. D., Froidevaux, L., Livesey, N. J., and Waters, J. W.: A study of stratospheric chlorine partitioning based on new satellite measurements and modeling, J. Geophys.. Res., 113, D12307, doi:10.1029/2007JD009057, 2008.

Santee, M. L., Manney, G. L., Livesey, N. J., Froidevaux, L., Schwartz, M. J., and Read, W. G.: Trace gas evolution in the lowermost stratosphere from Aura Microwave Limb Sounder measurements, J. Geophys. Res., 116, D18306, doi:10.1029/2011jd015590, 2011.

Solomon, S., Garcia, R. R., Rowland, F. S., and Wuebbles, D. J.: On the depletion of Antarctic ozone, Nature, 321, 755-758, 1986.

Solomon, S., Borrmann, S., Garcia, R. R., Portmann, R., Thomason, L., Poole, L. R., Winker, D., and McCormick, M. P.: Heterogeneous chlorine chemistry in the tropopause region, J. Geophys. Res., 102, 21,411-21,429, 1997.

Solomon, S.: Stratospheric ozone depletion: A review of concepts and history, Rev. Geophys., 37, 275-316, doi:10.1029/1999RG900008, 1999

Solomon, S., Kinnison, D., Bandoro, J., and Garcia, R.: Simulation of polar ozone depletion: An update, J. Geophys. Res., 120, 7958-7974, doi:10.1002/2015JD023365, 2015.

Solomon, S., Ivy, D. J., Kinninson, D., Mills, M. J., Neely III, R. R., and Schmidt, A.: Emergene of healing in the Antarctic ozone layer, Science, doi:10.1126/science.aae0061, 2016.

SPARC CCMVal: SPARC Report on the Evaluation of Chemistry–Climate Models, V. Eyring, T. G. Shepherd, and D. W. Waugh (Eds.), SPARC Report No.5, WCRP–132, WMO/TD–No.1526, 2010.

Sugita, T., Nakajima, H., Yokota, T., Kanzawa, H., Gernandt, H., Herber, A., von der Gathen, P., König-Langlo, G., Sato, K., Dorokhov, V., Yushkov, V. A., Murayama, Y., Yamamori, M., Godin-Beekmann, S., Goutail, F., Roscoe, H. K., Deshler, T., Yela, M., Taalas, P., Kyrö, E., Oltmans, S. J., Johnson, B. J., Allaart, M., Litynska, Z., Klekociuk, A., Andersen, S. B., Braathen, G. O., De Backer, H., Randall, C. E., Bevilacqua, R. M., Taha, G., Thomason, L. W., Irie, H., Ejiri, M. K., Saitoh, N., Tanaka, T., Terao, Y., Kobayashi, H., and Sasano, Y.: Ozone profiles in the high-latitude stratosphere and lower mesosphere measured by the Improved Limb Atmospheric Spectrometer (ILAS)-II: Comparison with other satellite sensors and ozonesondes, J. Geophys. Res., 111, D11S02, doi:10.1029/2005jd006439, 2006.

Tomikawa, Y., and Sato, K.: Trapped waves in the edge region of stratospheric polar vortices, J. Geophys. Res., 108, 4047, doi:10.1029/2002JD002579, 2003.

Tomikawa, Y., Sato, K., Hirasawa, N., Tsutsumi, M., and Nakamura, T.: Balloon-borne observations of lower stratospheric water vapor at Syowa Station, Antarctica in 2013, Polar Sci., 9, 345–353, doi:10.1016/j.polar.2015.08.003, 2015.

von Clarmann, T. and Johansson, S.: Chlorine nitrate in the atmosphere, Atmos. Chem. Phys., 18, 15,363-15,386, doi:10.5194/acp-18-15363-2018, 2018.

von Clarmann, T., Fischer, H., Friedl-Vallon, F., Linden, A., Oelhaf, H., Piesch, C., Seefeldner, M., and Völker, W.: Retrieval of stratospheric O_3, HNO_3, and $ClONO_2$ profiles from 1992 MIPAS-B limb emission spectra: method, results and error analysis, J. Geophys. Res., 98, 20,495-20,506, 1993.

von Clarmann, T., Glatthor, N., Grabowski, U., Höpfner, M., Kellmann, S., Kiefer, M., Linden, A., Tsidu, G. M., Milz, M., Steck, T., Stiller, G. P., Wand, D. Y., and Fischer, H.: Retrieval of temperature and tangent altitude pointing from limb emission spectra recorded from space by the Michelson Interferometer for Passive Atmospheric Sounding (MIPAS), J. Geophys. Res., 108, 4736, doi:10.1029/2003JD003602, 2003.

Waters, J. W., et al.: The Earth Observing System Microwave Limb Sounder (EOS MLS) on the Aura satellite, IEEE Trans. Geosci. Remote Sens., 44, 1075-1092, 2006.

Wegner, T., Grooß, J. -U., vonHobe, M. ,Stroh, F., Sumińska-Ebersoldt, O., Volk, C. M., Hösen, E., Mitev, V., Shur, G., and Müller, R.: Heterogeneous chlorine activ-ation on stratospheric aerosols and clouds in the Arctic polar vortex, Atmos. Chem. Phys., 12, 11,095-11,106, doi:10.5194/acp-12-11095-2012, 2012.

Winker, D. M., McGill, M., and Hunt, W. H.: Initial performance assessment of CALIOP, Geophys. Res. Lett., 34, L19803, doi:10.1029/2007GL30135, 2007.

WMO: Scientific Assessment of Ozone Depletion: 2006, Global Ozone Research and Monitoring Project—Report No. 50, 572 pp., Geneva, Switzerland, 2007.

WMO: Scientific Assessment of Ozone Depletion: 2010, Global Ozone Research and Monitoring Project—Report No. 52, 516 pp., Geneva, Switzerland, 2011.

WMO: Scientific Assessment of Ozone Depletion: 2014, Global Ozone Research and Monitoring Project—Report No. 55, 416 pp., Geneva, Switzerland, 2014.

WMO: Scientific Assessment of Ozone Depletion: 2018, Global Ozone Research and Monitoring Project—Report No. 58, 590 pp., Geneva, Switzerland, 2019.

Wood, S. W., Bodeker, G. E., Boyd, I. S., Jones, N. B., Connor, B. J., Johnston, P. V., Matthews, W. A., Nichol, S. E., Murcray, F. J., Nakajima, H., and Sasano, Y.: Validation of version 5.20 ILAS HNO_3, CH_4, N_2O, O_3, and NO_2 using ground-based measurements at Arrival Heights and Kiruna, J. Geophys. Res., 107, 8208, doi:10.1029/2001jd000581, 2002.

Wood, S. W., Batchelor, R. L., Goldman, A., Rinsland, C. P., Connor, B. J., Murcray, F. J., Stephen, T. M., and Heuff, D. N.: Ground-based nitric acid measurements at Arrival Heights, Antarctica, using solar and lunar Fourier transform infrared observations, J. Geophys. Res., 109, D18307, doi:10.1029/2004jd004665, 2004.

Yang, E.-S., Cunnold, D. M., Newchurch, M. J., Salawitch, R. J., McCormick, M. P., Russell III, J. M., Zawodny, J. M., and Oltmans, S. J.: First stage of Antarctic ozone recovery, J. Geophys.. Res., 113, D20308, doi:10.1029/2007JD009675, 2008.

Ziemke, J. R., Chandra, S., Labow, G. J., Bhartia, P. K., Froidevaux, L., and Witte, J. C.: A global climatology of tropospheric and stratospheric ozone derived from Aura OMI and MLS measurements, Atmos. Chem. Phys., 11, 9237-9251, doi:10.5194/acp-11-9237-2011, 2011.

Tables

Table 1. FTIR observation dates at Syowa Station in 2007 and 2011

Month	Dates (2007)	Dates (2011)	Number of days inside the polar vortex (2007/2011)	Number of days in the boundary region of the polar vortex (2007/2011)	Number of days outside the polar vortex (2007/2011)	Number of measurement days (2007/2011)
March	25		0 / 0	0 / 0	1 / 0	1 / 0
April	1, 3, 4, 5, 8, 24, 26, 28		0 / 0	0 / 0	8 / 0	8 / 0
May	8, 9, 10, 13, 14, 15, 20, 21, 22		7 / 0	0 / 0	2 / 0	9 / 0
June			0 / 0	0 / 0	0 / 0	0 / 0
July	29, 30		0 / 0	2 / 0	0 / 0	2 / 0
August	1, 8, 9, 10, 24, 25, 26, 28, 29		8 / 0	1 / 0	0 / 0	9 / 0
September	1, 4, 5, 6, 7, 8, 16, 18, 23, 26, 27, 30	25, 29, 30	12 / 3	0 / 0	0 / 0	12 / 3
October	6, 10, 11, 14, 19, 20, 25, 26, 27	1, 3, 4, 8, 11, 22, 23, 24, 26	9 / 9	0 / 0	0 / 0	9 / 9
November	2, 3, 5, 6, 7, 8, 9, 10, 11, 16, 17, 18, 19, 21, 27, 29, 30	1, 2, 3, 9, 11, 16, 19	12 / 7	1 / 0	4 / 0	17 / 7
December	4, 7, 8, 9, 13, 15, 16, 17, 20, 22, 29		8 / 0	0 / 0	3 / 0	11 / 0
Total			56 / 19	4 / 0	18 / 0	78 / 19

Table 2. Retrieval parameters of SFIT2

Species	O_3	HNO_3	HCl
Spectroscopy	HITRAN 2008	HITRAN 2008	HITRAN 2008
PT Profile	Daily sonde (0-30 km) CIRA 86 (30-100 km)	Daily sonde (0-30 km) CIRA 86 (30-100 km)	Daily sonde (0-30 km) CIRA 86 (30-100 km)
A priori profiles	Monthly averaged by ozonesonde (0-30 km) & ILAS-II (30-100 km)	Monthly averaged by ILAS-II	Monthly averaged by HALOE
Microwindows (cm^{-1})	1002.578 – 1003.500 1003.900 – 1004.400 1004.578 – 1005.000	867.000 – 869.591 872.800 – 874.000	2727.730 – 2727.830 2775.700 – 2775.800 2925.800 – 2926.000
Retrieved interfering species	O_3 (668), O_3 (686), CO_2, H_2O	H_2O, OCS, NH_3, CO_2, C_2H_6	CO_2, H_2O, O_3, NO_2

Table 3. Summary of validation results of FTIR profiles compared with ozonesonde and Aura/MLS measurements, and possible Aura/MLS biases from literatures

	D (%) 18-22 km	Min/Max (%) 18-22 km	Agreement 15-25 km (ppmv/ppbv)	Literature values
O_3	+6.2	-10.4/+19.2	-0.02~+0.40	
HNO_3	+13.2	+0.2/+21.9	-0.56~+0.57	Aura/MLS no bias with errors (0.6 ppbv) (Livesey et al., 2011)
HCl	-9.7	-14.6/-3.0	-0.2~+0.09	Aura/MLS > HALOE by 10-15%, precision 0.2-0.6 ppbv (Livesey et al., 2013)

Table 4. Summary of minor atmospheric species variations

Altitude	18 km		22 km	
Year	2007	2011	2007	2011
ClO enhanced period (day)	230-260	230-260	220-240	230-250
Variation when ClO enhanced (ppbv)	0–1.3	0–1.5	0–2.2	0–2.2
HCl value before winter (ppbv)	1.5–1.8	1.2–1.6	2.1–2.4	1.8–2.2
HCl starting-ending day of decrease (day)	140-180	140-180	130-180	140-170
Variation when HCl ~ 0 (ppbv)	0–0.3	0–0.3	0.1–1.0	0.1–0.9
HCl starting-ending day of increase (day)	250-300	250-300	240-280	240-300
HCl Value after increase (ppbv)	2.6–3.0	2.5–2.8	2.1–2.4	2.0–2.5
HCl Value outside polar vortex (ppbv)	1.5–2.0	1.0–1.8	1.5–2.0	1.5–2.0
$ClONO_2$ Value before winter (ppbv)	~0.5	~0.4	0.6–0.9	0.6–0.7
Variation when $ClONO_2$~0 (ppbv)	0–1.5	0–1.5	0–2.0	0–2.0
Day of $ClONO_2$ enhancement	-	270-300	270-280	270–280
Value of $ClONO_2$ enhancement (ppbv)	-	1.5	1.5	1.5
$ClONO_2$ value after enhancement (ppbv)	0–0.3	0–0.2	0.8–1.3	0.8–1.1
$ClONO_2$ value outside polar vortex (ppbv)	0.3–0.4	0.2–0.3	0.5–0.7	0.6–0.8
O_3 value before winter (ppmv)	2.5	2.5	4.0	4.0
O_3 starting-ending day of decrease (day)	190-280	200-270	170-260	170-270
O_3 minimum value (ppmv)	0.3	0.5	2.0	1.0
O_3 value after recovery (ppmv)	0.8	0.8	2.4–4.0	2.0–3.5
HNO_3 value before winter (ppbv)	6-10	8-10	15-16	13–15
HNO_3 starting-ending day of decrease (day)	160-190	150-180	140-180	150-180
HNO_3 minimum value (ppbv)	0	0	2	1
HNO_3 value after recovery (ppbv)	3–4	3–4	4–6	4–5

* ‘ClO enhanced period’ is defined as the period when ClO values were more than 80 % of its maximum value.

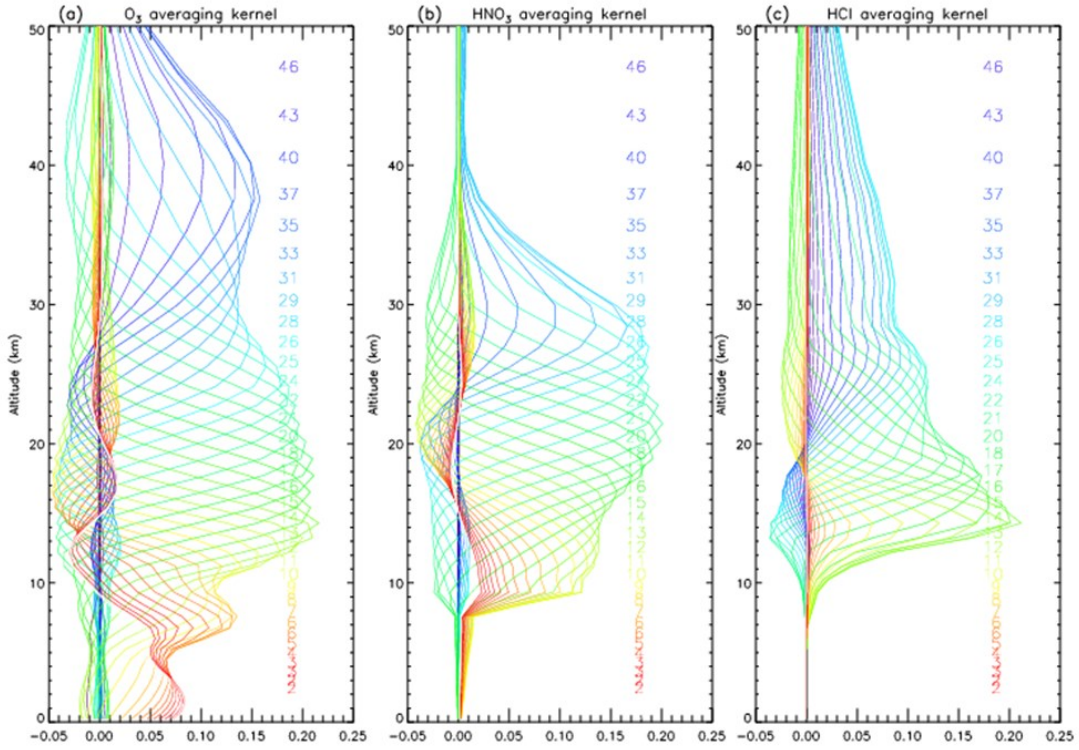

Figure 1. Averaging kernel functions of the SFIT2 retrievals for O_3 (a), HNO_3 (b), and HCl (c).

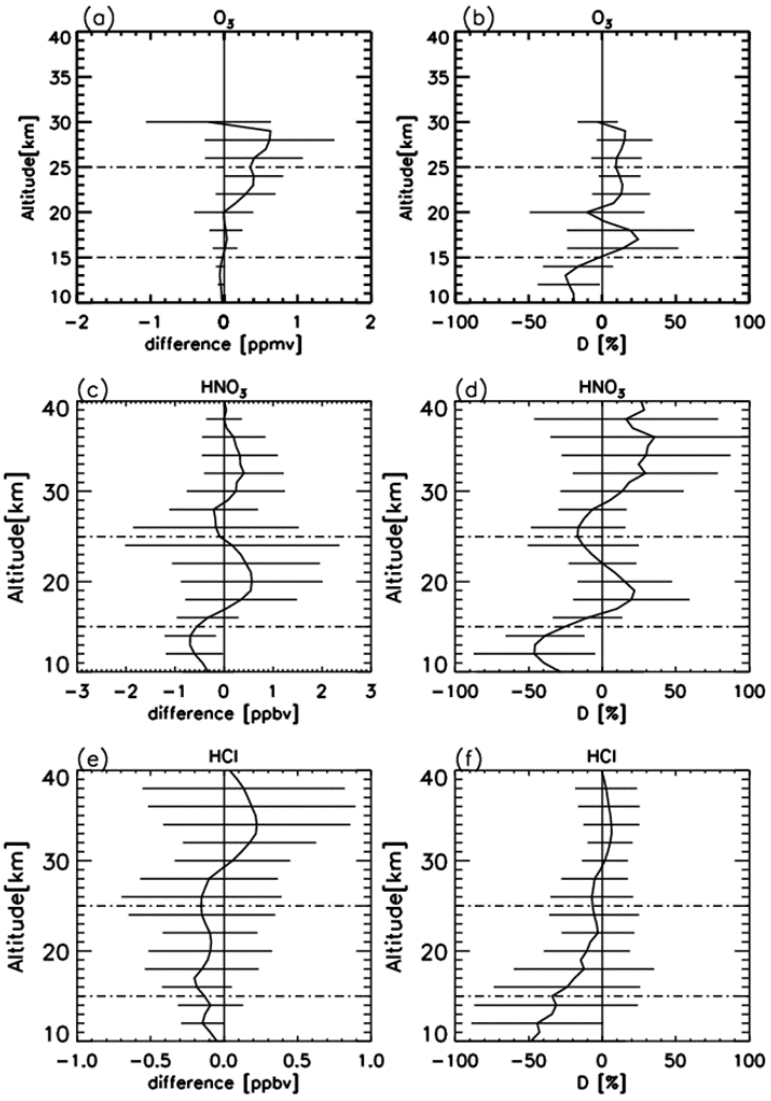

Figure 2. Absolute (a) and percentage (b) differences of O_3 profiles retrieved from FTIR measurements and those from ozonesonde measurements. Horizontal bars indicate the standard deviation of differences at each altitude. Absolute (c) and percentage (d) differences of HNO_3 profiles retrieved from FTIR measurements and those from Aura/MLS measurements. Absolute (e) and percentage (f) differences of HCl profiles retrieved from FTIR measurements and those from Aura/MLS measurements.

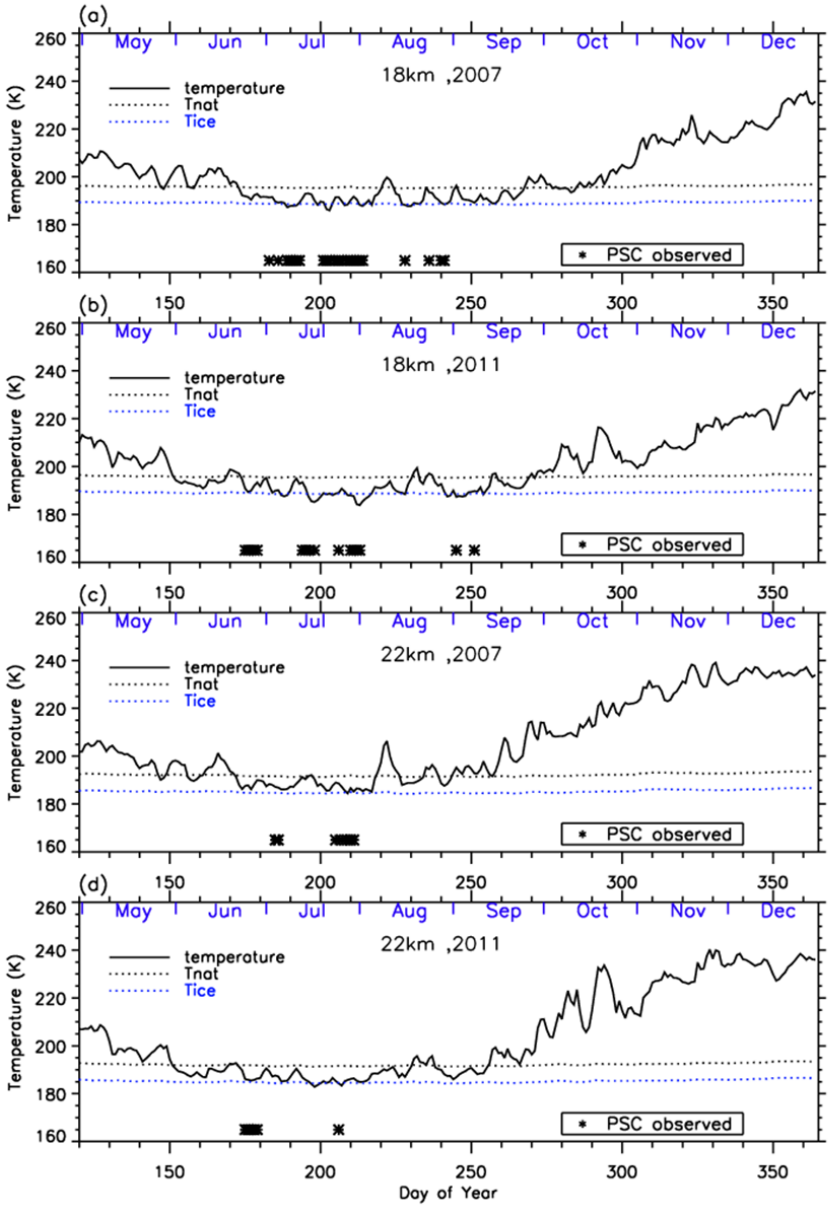

Figure 3. Time series of temperatures at 18 km in (a) 2007 and (b) 2011, and at 22 km in (c) 2007 and (d) 2011 over Syowa Station using ERA-Interim data. Approximate saturation temperatures for nitric acid trihydrate PSC (T_{NAT}) and ice PSC (T_{ICE}) calculated by assuming 6 ppbv HNO_3 and 4.5 ppmv H_2O are also plotted in the figures by dotted lines. Dates when PSCs were observed over Syowa Station are indicated by asterisks on the bottom of the figures.

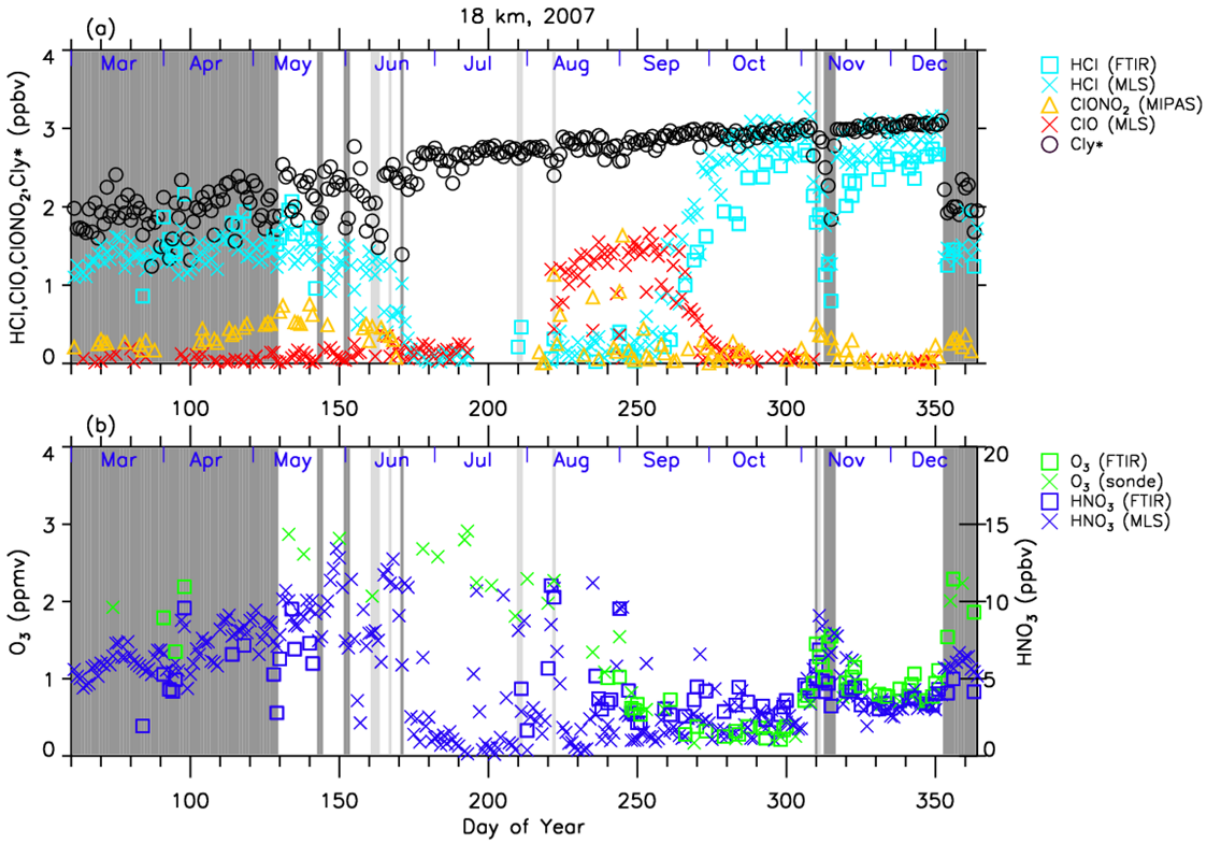

Figure 4. Time series of (a) HCl, $ClONO_2$, ClO, Cl_y*, (b) O_3, and HNO_3 mixing ratios at 18 km in 2007 over Syowa Station. O_3(FTIR), HCl(FTIR), and HNO_3(FTIR) were measured by FTIR at Syowa Station, while HCl(MLS), ClO(MLS), and HNO_3(MLS) were measured by Aura/MLS. O_3(sonde) was measured by ozonesonde. $ClONO_2$ was measured by Envisat/MIPAS. Cl_y* is calculated from N_2O value. See text in detail. The unit of O_3 is ppmv and the other gases are ppbv. The dark shaded area, the light shaded area, and the white area indicate the days when Syowa Station was located outside, in the boundary region, and inside the polar vortex, respectively.

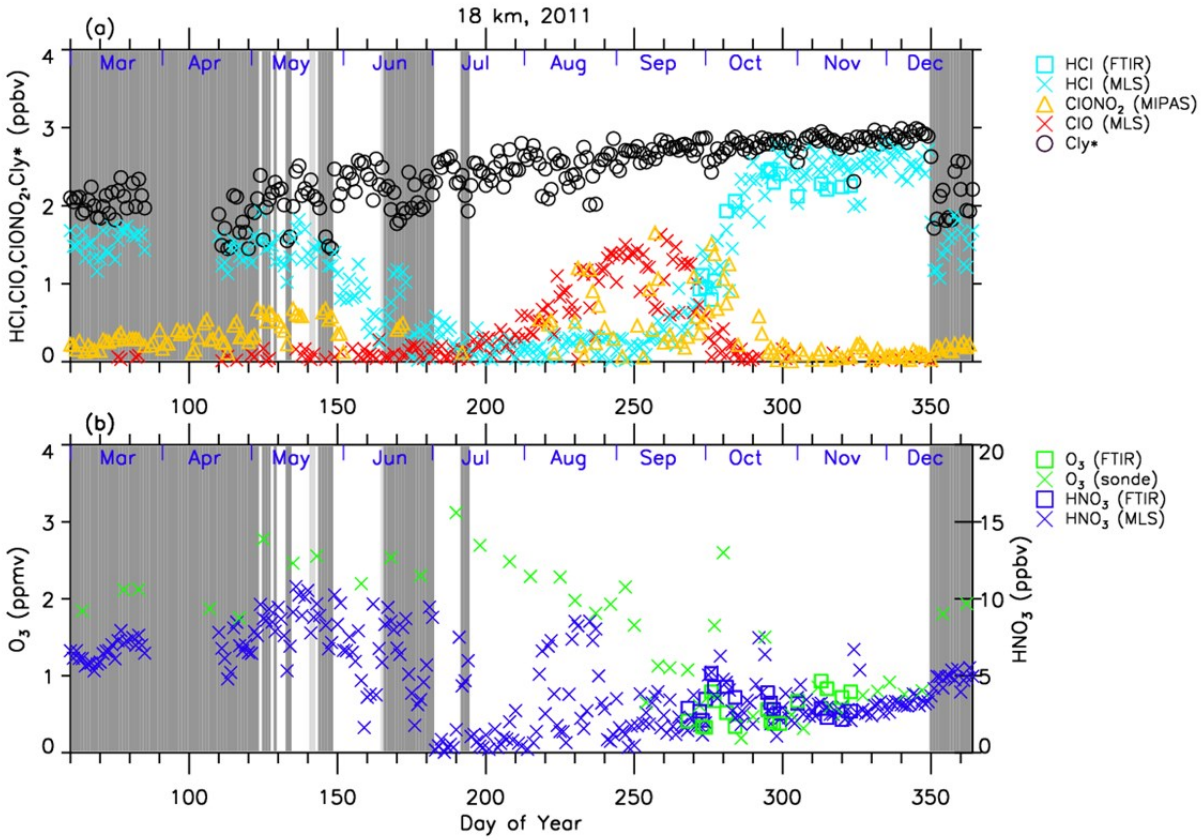

Figure 5. Same as Figure 4 but in 2011.

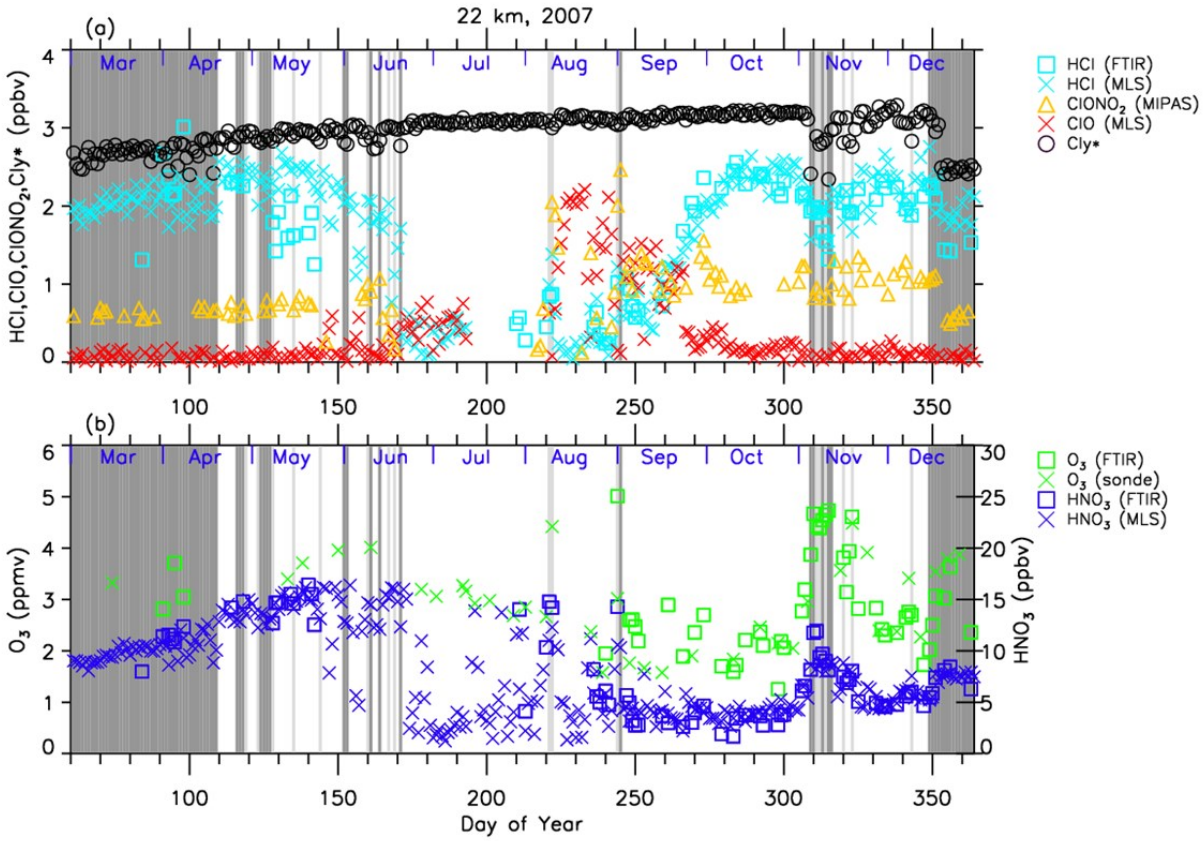

Figure 6. Same as Figure 4 but at 22 km.

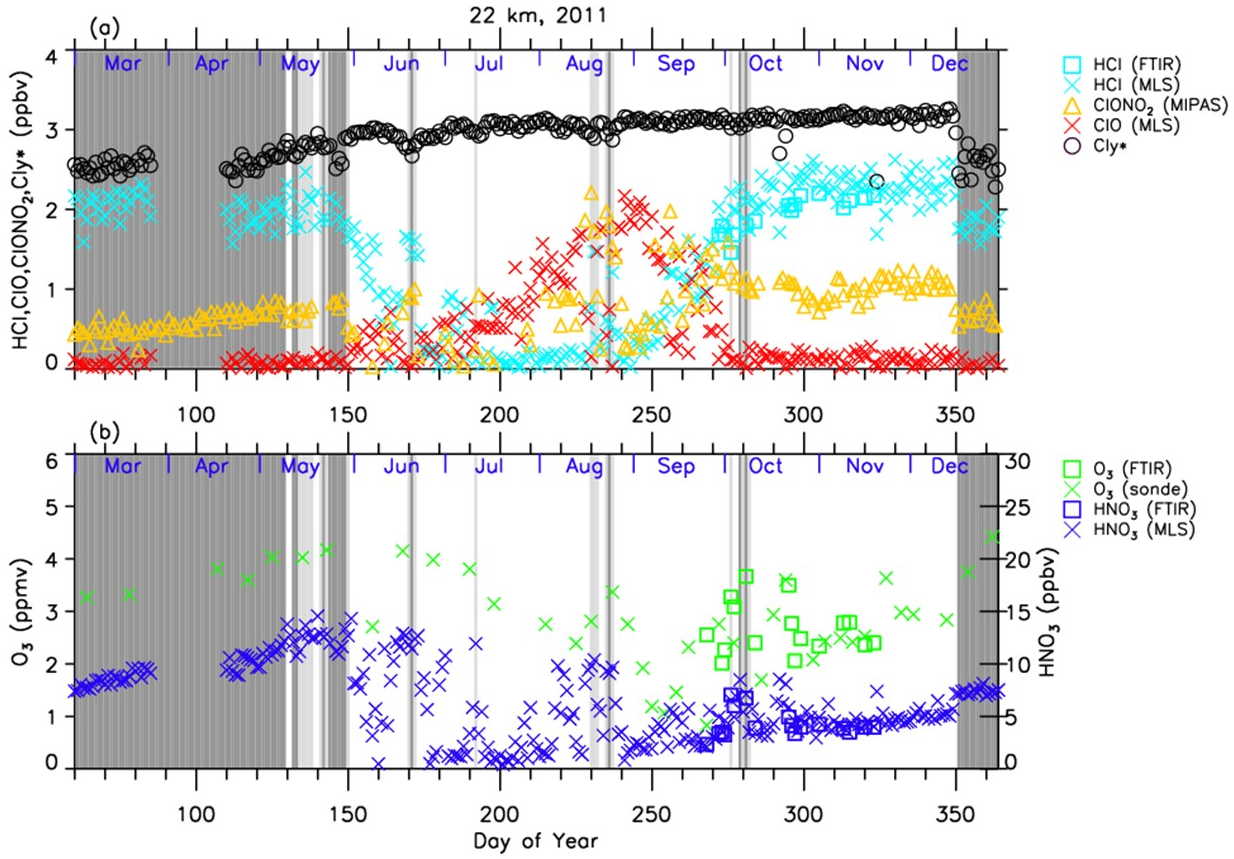

Figure 7. Same as Figure 5 but at 22 km.

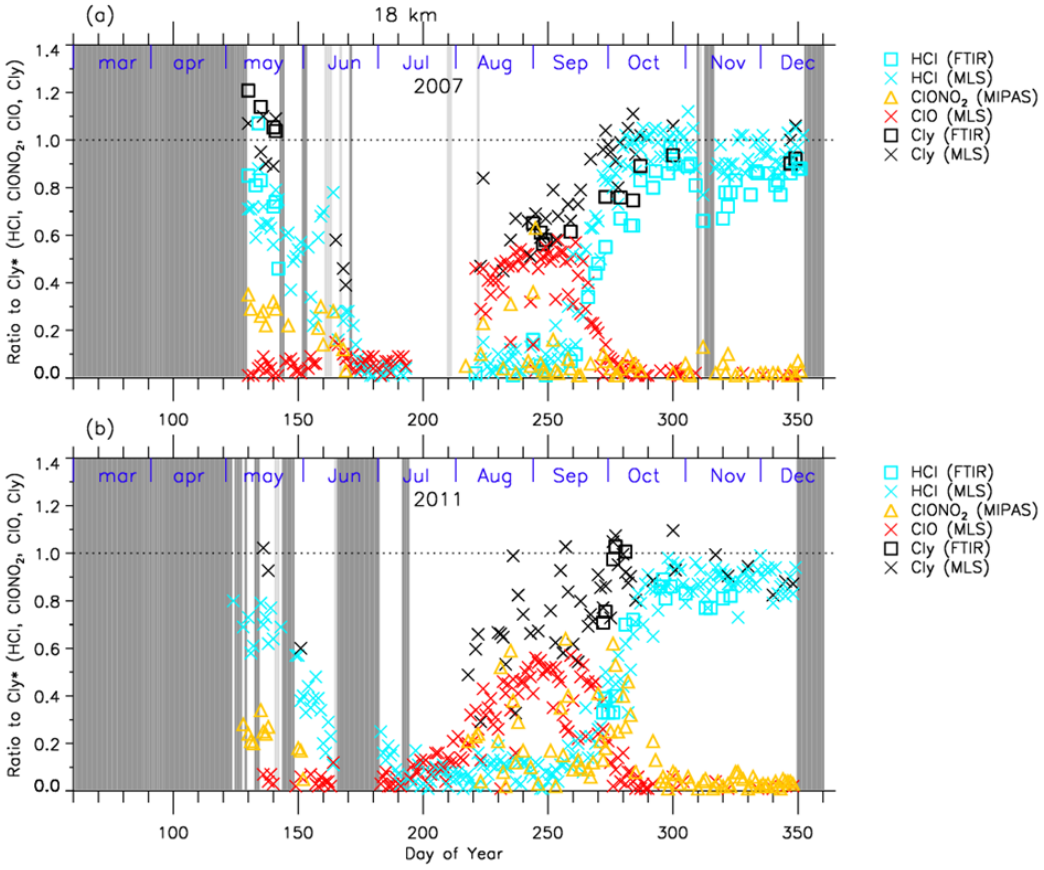

Figure 8. Time series of the ratios of HCl, $ClONO_2$, ClO, and Cl_y(=HCl+$ClONO_2$+ClO) to total chlorine (Cl_y*) over Syowa Station at 18 km in (a) 2007 and in (b) 2011. Shaded areas are the same as Figure 4.

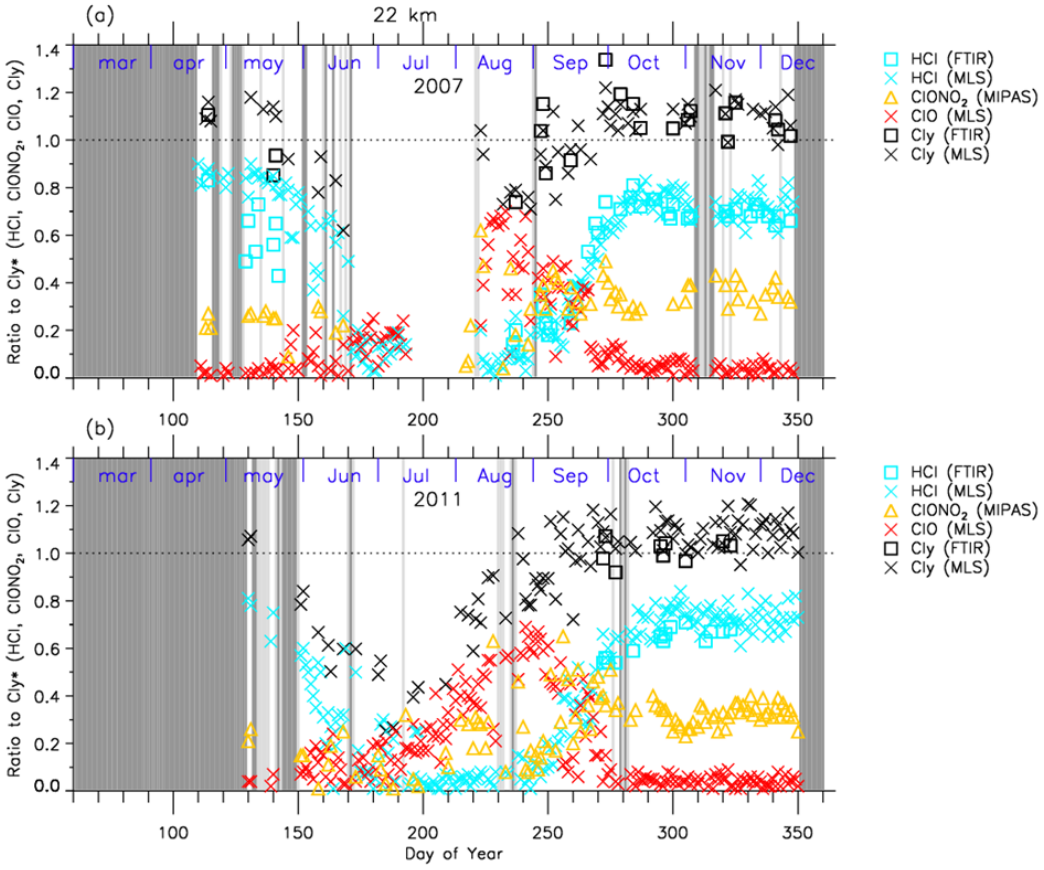

Figure 9. Same as Figure 8 but at 22 km.

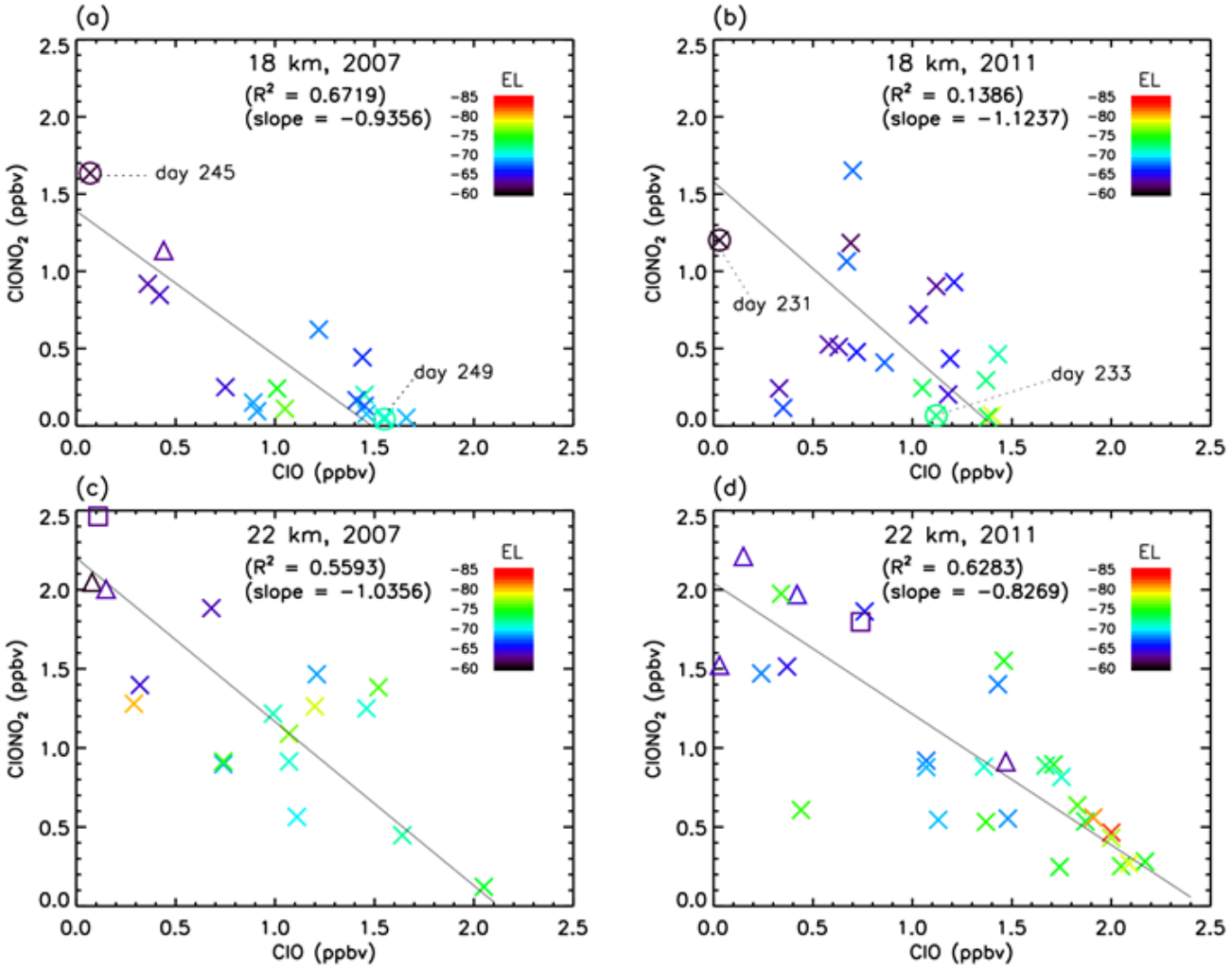

Figure 10. Scatter plot between ClO (Aura/MLS) and $ClONO_2$ (Envisat/MIPAS) mixing ratios between August 8 and September 17 (day 220 – 260) at 18 km and 22 km in 2007 and 2011. Crosses, triangles, and squares represent the data when Syowa Station was located inside the polar vortex, the boundary region, and outside the polar vortex, respectively. Solid lines are regression lines obtained by RMA (Reduced Major Axis) regression. Color represents the equivalent latitude over Syowa Station on that day. Circles with crosses represent the days which are shown in Figures 13 and 14.

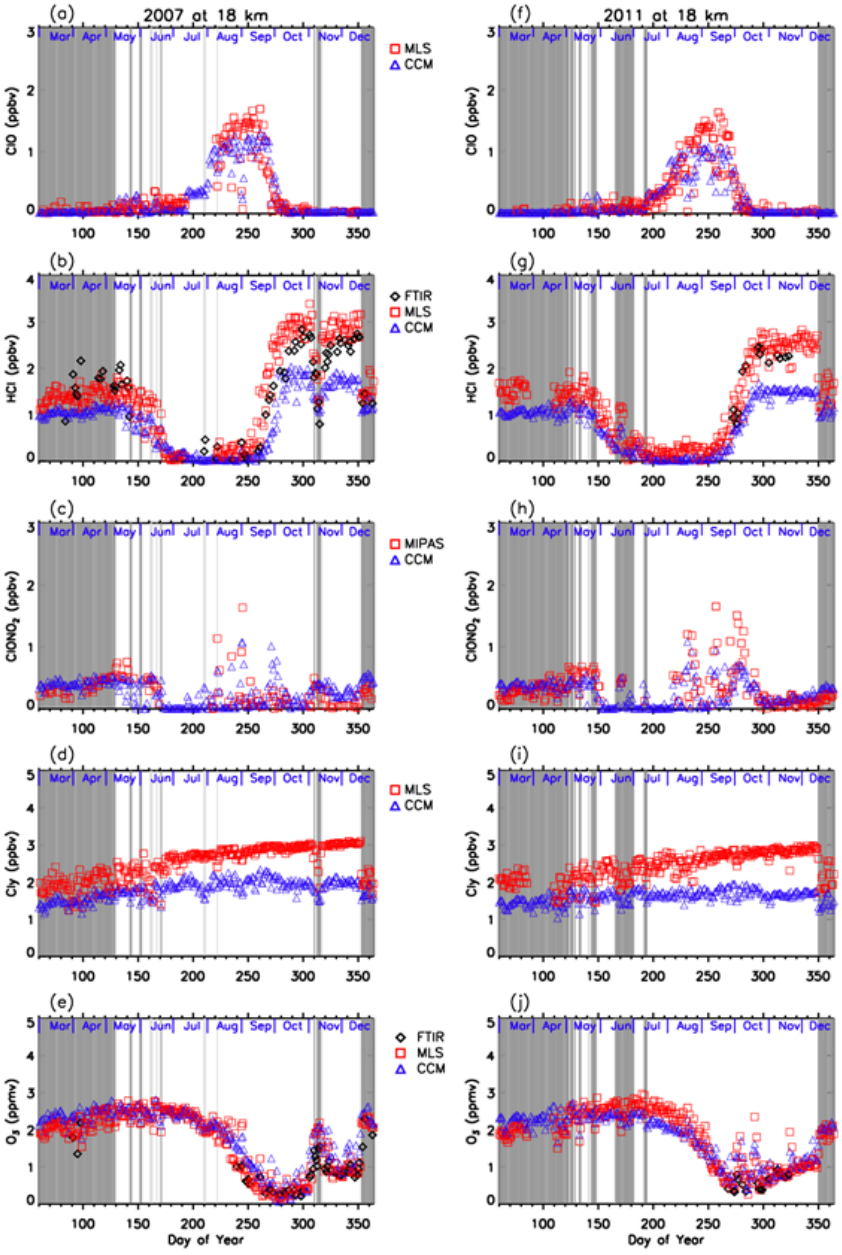

Figure 11. Daily time series of measured and modeled minor species over Syowa Station at 18 km. Black diamonds are data by FTIR, red squares are by Aura/MLS and Envisat/MIPAS, blue triangles are data by MIROC3.2 CCM. (a) is for ClO, (b) is for HCl, (c) is for $ClONO_2$, (d) is for Cly, and (e) is for O_3 in 2007. (f) is for ClO, (g) is for HCl, (h) is for $ClONO_2$, (i) is for Cly, and (j) is for O_3 in 2011.

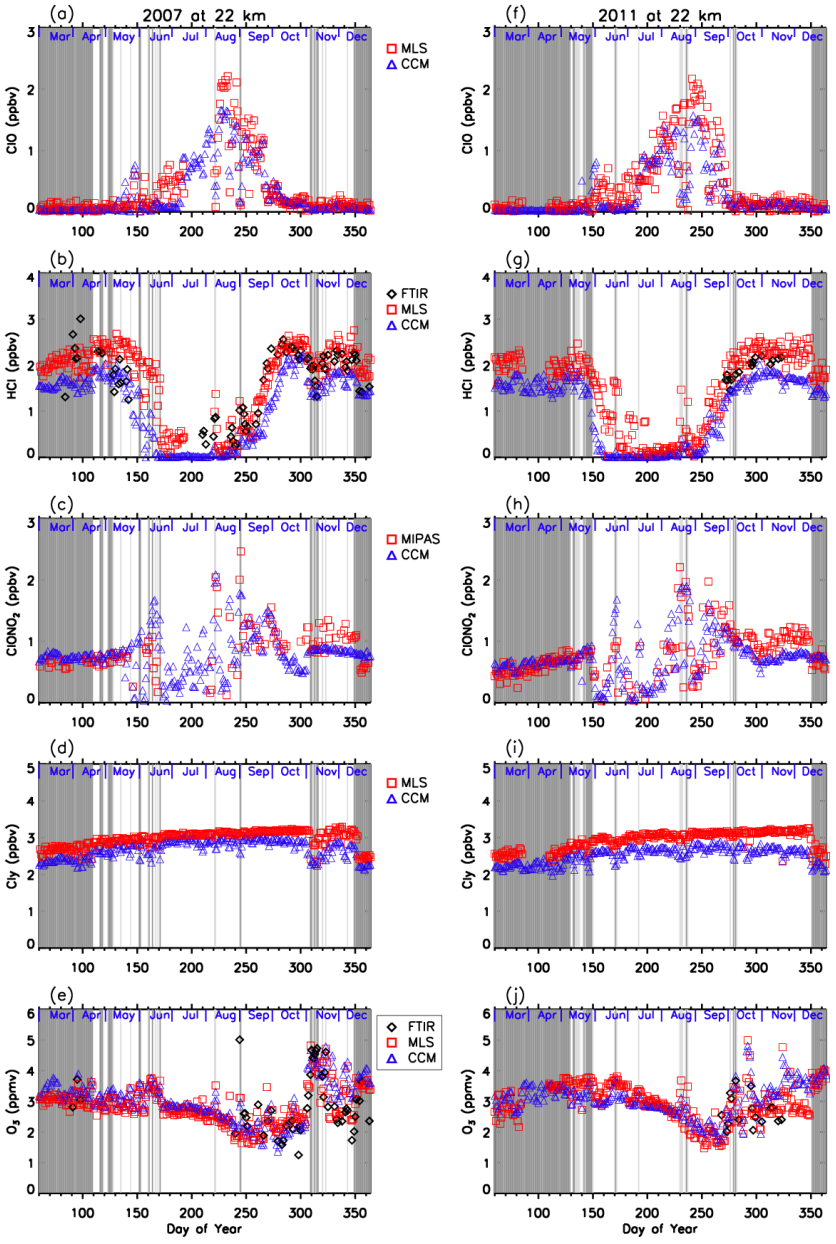

Figure 12. Same as Figure 11 but for 22 km.

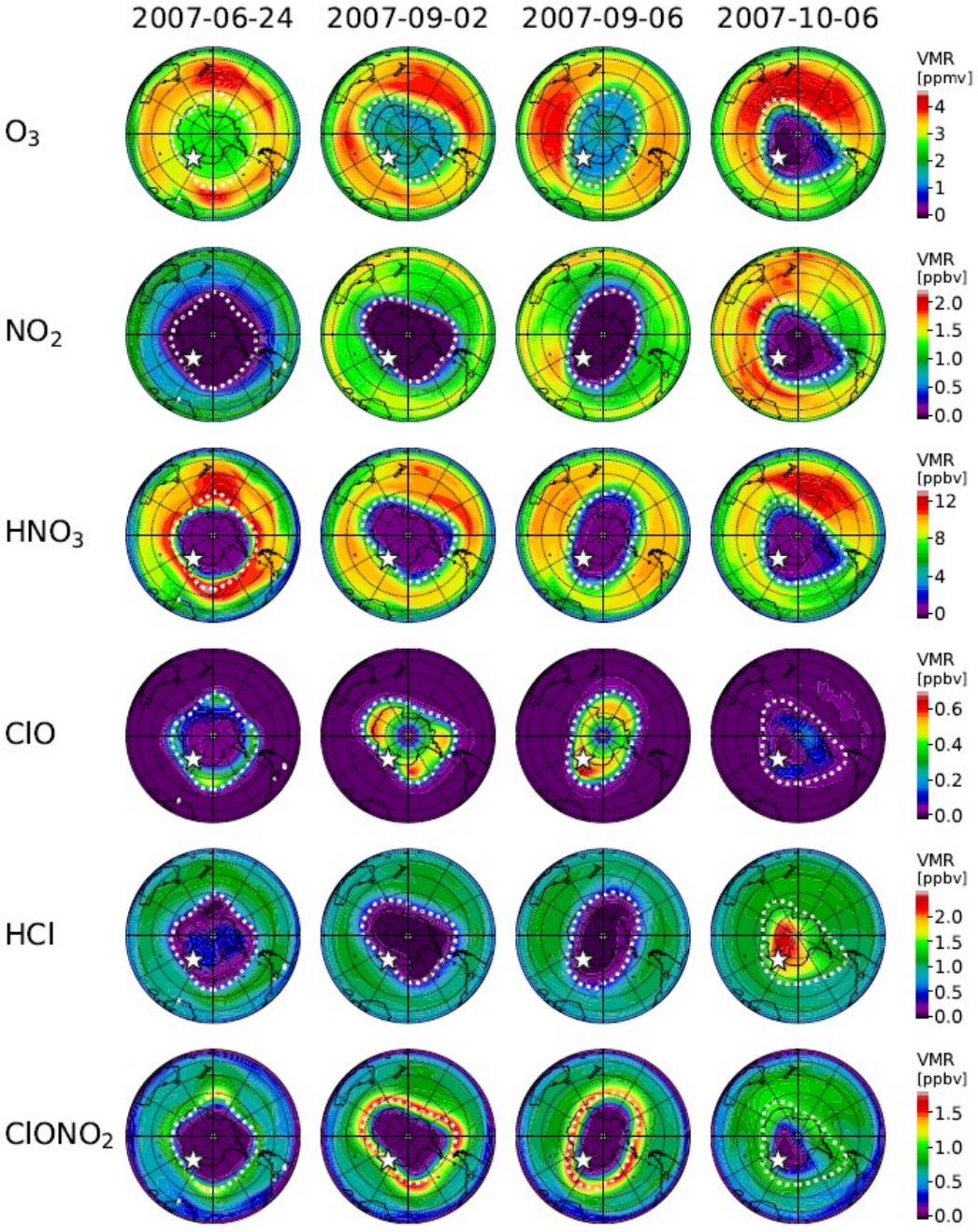

Figure 13. Polar southern hemispheric plot for simulated mixing ratios of O_3, NO_2, HNO_3, ClO, HCl, and $ClONO_2$ by a MIROC3.2 chemistry-climate model (CCM) at 50 hPa for June 24 (day 175), September 2 (day 245), September 6 (day 249), and October 6 (day 279), 2007. Polar vortex boundary at 475 K calculated from ERA-Interim reanalysis data was plotted by dotted circle in each pane. The location of Syowa Station is shown by white star in each panel.

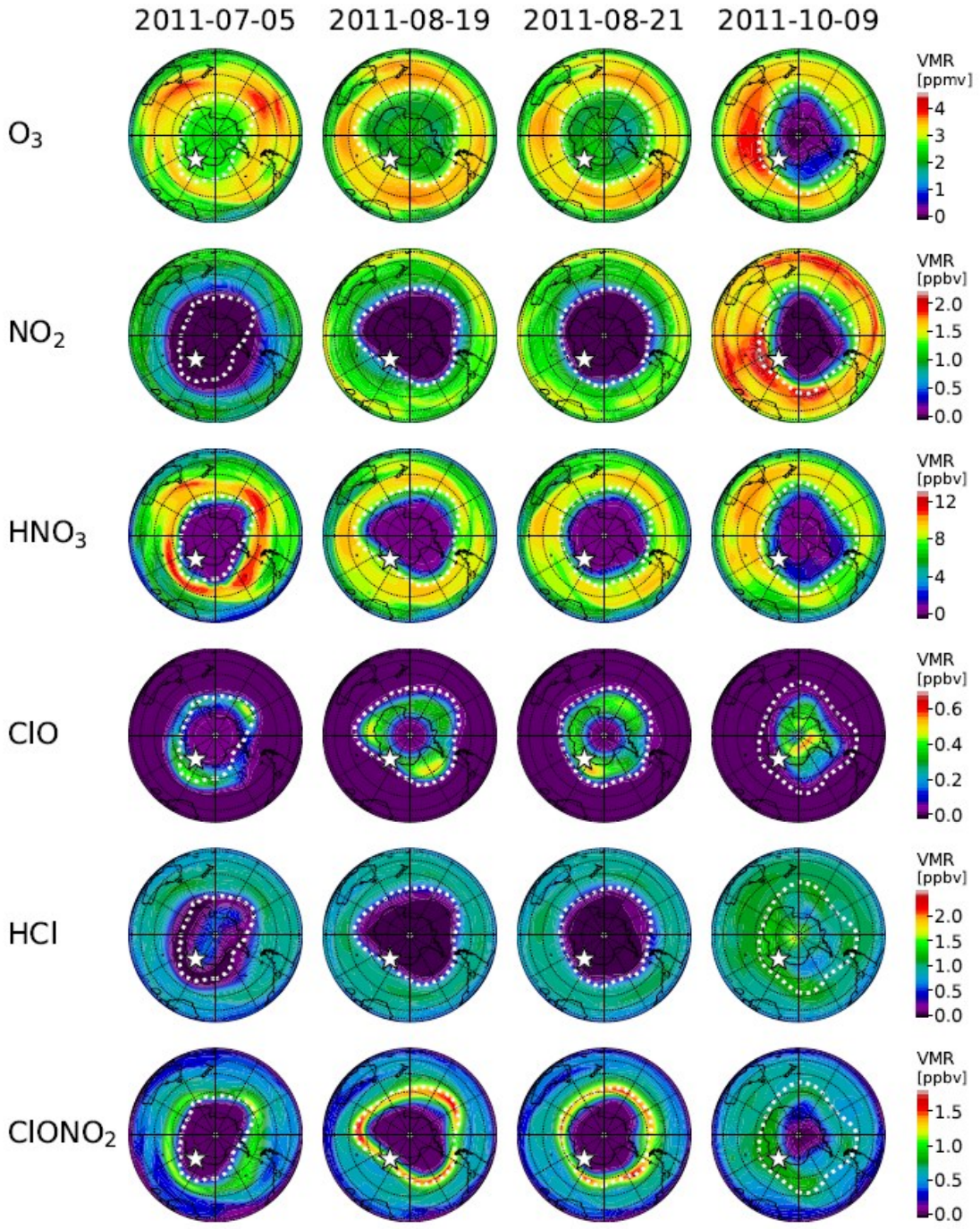

Figure 14. Same as Figure 13 but for July 5 (day 186), August 19 (day 231), August 21 (day 233), and October 9 (day 282), 2011.

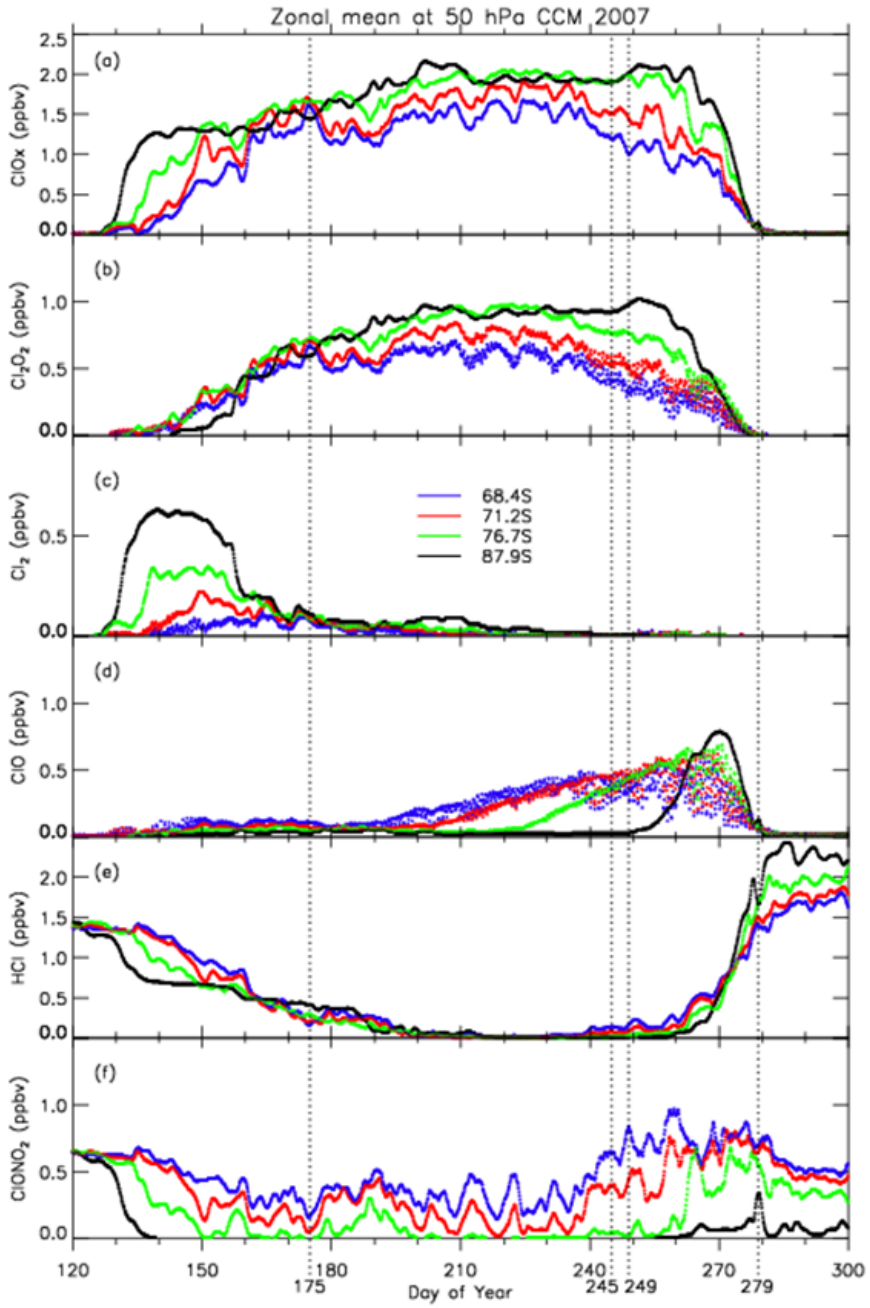

Figure 15. Three-hourly zonal-mean time series of MIROC3.2 CCM outputs for (a) $ClO+2*Cl_2O_2+2*Cl_2$, (b) Cl_2O_2, (c) Cl_2, (d) ClO, (e) HCl, and (d) $ClONO_2$ during day number 120–300 at 50 hPa in 2007.